

Prospects for measuring quark polarization and spin correlations in $b\bar{b}$ and $c\bar{c}$ samples at the LHC

Yevgeny Kats and David Uzan

Department of Physics, Ben-Gurion University, Beer-Sheva 8410501, Israel

E-mail: katsye@bgu.ac.il, daviduz@post.bgu.ac.il

ABSTRACT: Polarization and spin correlations have been studied in detail for top quarks at the LHC, but have been explored very little for the other flavors of quarks. In this paper we consider the processes $pp \rightarrow q\bar{q}$ with $q = b, c$ or s . Utilizing the partial preservation of the quark's spin information in baryons in the jet produced by the quark, we examine possible analysis strategies for ATLAS and CMS to measure the quark polarization and spin correlations. We find polarization measurements for the b and c quarks to be feasible, even with the currently available datasets. Spin correlation measurements for $b\bar{b}$ are possible using the CMS Run 2 parked data, while such measurements for $c\bar{c}$ will become possible with higher integrated luminosity. For the s quark, we find the measurements to be challenging with the standard triggers. We also provide leading-order QCD predictions for the polarization and spin correlations expected in the $b\bar{b}$ and $c\bar{c}$ samples with the cuts envisioned for the above analyses. Apart from establishing experimentally the existence of spin correlations in $b\bar{b}$ and $c\bar{c}$ systems produced in pp collisions, the proposed measurements can provide new information on the polarization transfer from quarks to baryons and might even be sensitive to physics beyond the Standard Model.

Contents

1	Introduction	2
2	Polarization Retention in Baryons	3
3	Baryon Production and Relevant Decay Channels	4
4	Polarization and Spin Correlations	7
4.1	Quark-Antiquark Pair Spin State Description	7
4.2	Decay Angular Distributions	9
4.3	Statistical Uncertainty Evaluation	11
5	Quark Polarization and Spin Correlations in QCD	12
6	Proposed Analyses and Their Prospects	13
6.1	Benchmark Datasets	14
6.2	Analyses of $pp \rightarrow s\bar{s}$	15
6.2.1	Λ Reconstruction, Efficiency and Signal Yield	16
6.2.2	Background	17
6.2.3	Measurement prospects	17
6.3	Analyses of $pp \rightarrow c\bar{c}$	18
6.3.1	Hadronic Channel	18
6.3.2	Semileptonic Channel	21
6.3.3	Mixed Channel	23
6.4	Analyses of $pp \rightarrow b\bar{b}$	26
6.4.1	Inclusive Selection	26
6.4.2	Exclusive Selection	29
6.4.3	Semi-inclusive Selection	32
6.4.4	Mixed Selections	33
6.4.5	CMS Parked Data	33
6.4.6	Expected Precision	34
7	Summary and Discussion	35
A	Statistical Uncertainty Formulas	39

1 Introduction

Quark polarization and spin correlations are properties that have been extensively researched for top quarks at the LHC, both theoretically (e.g., refs. [1–11]) and experimentally (e.g., refs. [12–17]), but have not yet been explored much for the b , c , or s quarks. Measurements of these quantities can provide interesting information on both Standard Model (SM) and Beyond the Standard Model (BSM) interactions. There exist proposals for methods to measure quark polarizations in samples of $pp \rightarrow t\bar{t}$, in which b quarks are available from the $t \rightarrow W^+b$ decay, and c and s quarks from the subsequent decay $W^+ \rightarrow \bar{s}c$ [18–20], and using samples of $pp \rightarrow W^-c$ for c quarks [21]. The b , c , and s quarks in these processes are expected to be highly polarized due to the electroweak interaction. On the other hand, in the current paper we want to examine quark-antiquark pair production, $pp \rightarrow q\bar{q}$, where q can be either b , c or s . These processes are dominated by QCD interactions, which produce the quarks unpolarized at the leading order. However, sizable spin correlations are expected, as we will quantify, similar to the top-quark case.

Unlike the top quark, whose spin information can be obtained from the angular distributions of its decay products, the b , c and s quarks are only observed as jets of hadrons, making it more challenging to obtain the spin information of the original quarks. It can nevertheless be done by measuring the polarization and spin correlations of baryons produced from these quarks. This approach was originally proposed for measuring the longitudinal polarization of the heavy quarks (b and c) produced in Z decays at LEP [22–24]. Such measurements were subsequently performed for the b quark using Λ_b baryons [25–27], confirming the expectation of a sizable polarization transfer from the b quark to the Λ_b . Analogous measurements have shown that the s -quark longitudinal polarization is preserved in Λ baryons that carry a significant fraction of the jet momentum [28–30]. This method to access quark spin information has been analyzed in the context of the LHC in refs. [18–21], where it was shown that a number of interesting measurements of longitudinal polarization of quarks produced in top-quark decays are possible even with the statistics of Run 2. In addition, attempts to measure the transverse polarization of Λ_b in inclusive QCD samples, which is expected to be small, have been reported by LHCb [31, 32] and CMS [33]. When moving to spin correlations, the cost in statistics increases significantly since the prices for the fragmentation to baryons, the branching ratios of the useful decays, and the reconstruction efficiency, are squared. It is therefore an example of analyses that will benefit from the increase in statistics offered by the high-luminosity phase of the LHC.

The spin correlation measurements will allow quantifying the effect of the polarization transfer from quarks to baryons for longitudinal polarization (cross-checking the information that would presumably be obtained even earlier in the analyses proposed in refs. [18, 19]) as well as transverse polarization. This will provide certain cross-grained information about the spin-dependent fragmentation functions [34, 35] of the b and c quarks hadronizing to the Λ_b and Λ_c baryons, respectively. Polarization and spin correlation measurements can also be sensitive to BSM contributions to $b\bar{b}$ or $c\bar{c}$ production. Similar ideas apply to $s\bar{s}$, but we will find the corresponding measurements to be challenging.

We will consider both the Run 2 and the High Luminosity LHC (HL-LHC) datasets

of ATLAS and CMS, including the CMS parked b -hadron dataset [36, 37]. The goal of the current paper is to do a broad survey of the possible analyses, considering a variety of baryon decay modes and selection schemes. We will therefore restrict ourselves to rough estimates of the expected sensitivity in each case, leaving more detailed simulations of individual analyses and the consideration of systematic uncertainties to future work. We also leave to future work the exploration of similar opportunities in LHCb. While limited in the integrated luminosity and acceptance, the LHCb detectors offer superior tracking and particle identification capabilities. It is therefore plausible that a complementary set of analyses, for low- p_T quarks, will be possible in LHCb. It should be noted, however, that the assumption of the factorization between the quark production and its hadronization can break down at low p_T , making the result interpretation difficult.

The rest of the paper is organized as follows. Section 2 reviews the essentials of quark polarization retention in baryons. Section 3 provides details on baryon production and discusses the baryon decay modes that will be relevant to us. Section 4 reviews the formalism for the description of polarization and spin correlations and presents the angular distributions through which these quantities can be measured. In section 5 we simulate the polarization and spin correlations for $b\bar{b}$ and $c\bar{c}$ expected in QCD after validating our simulation on $t\bar{t}$. In section 6, we describe the various possible analysis channels in detail, discuss the most important backgrounds in each case, and estimate the expected sample purity and measurement precision. We summarize the conclusions in section 7. Appendix A presents the derivation of formulas for the statistical uncertainties of the polarization and spin correlation measurements.

2 Polarization Retention in Baryons

For the heavy quarks, namely b and (to some extent) c , the polarization is expected to be preserved through the hadronization (on timescales of order $1/\Lambda_{\text{QCD}}$) [22–24]. This happens since $m_q \gg \Lambda_{\text{QCD}}$ implies that the effect on the heavy quark spin via the chromomagnetic dipole moment, which scales as $\mu_q \propto 1/m_q$, is negligible.

If the heavy quark q ($= b$ or c) ends up in a Λ_q baryon, the baryon polarization is approximately equal to the quark polarization. It is so because the Λ_q structure in the framework of the quark model is qud with the u and d forming a spin singlet, so all the spin is on the q . If, on the other hand, the q ends up in a Σ_q or Σ_q^* baryon, which are analogous to the Λ_q but with the light quarks forming a spin and isospin triplet, the Λ_q baryons produced in $\Sigma_q^{(*)} \rightarrow \Lambda_q \pi$ decays will not carry the same polarization as the original quark [24]. The Λ_q from these decay channels are hard to distinguish from the direct Λ_q production and thus they lower the polarization retention. Due to similar reasons, it is essentially impossible to extract polarization information from meson decays [24, 38].

The polarization loss effect due to the contamination of the Λ_q sample with $\Sigma_q^{(*)} \rightarrow \Lambda_q \pi$ decays has been analyzed in refs. [18, 24] and it was found that the inclusive Λ_q samples end up carrying between roughly 50% and 80% of the original quark polarization, and this number may differ between the cases of longitudinal and transverse polarization (with respect to the fragmentation axis). In the current paper we will not repeat the discussions

on the various approaches to estimating these effects but only parameterize them in terms of the longitudinal and transverse *polarization retention factors*, r_L and r_T , defined as

$$r_{\hat{\mathcal{P}}} = \frac{\mathcal{P}(\Lambda_q)}{\mathcal{P}(q)}, \quad (2.1)$$

where \mathcal{P} denotes polarization and $\hat{\mathcal{P}} = L$ or T denotes whether its direction is longitudinal or transverse with respect to the fragmentation axis. We also note that r_L for bottom and charm quarks can be measured by ATLAS and CMS in their Run 2 $t\bar{t}$ samples [18], and for charm quarks possibly also in $W+c$ samples [21]. Measurements of both r_L and r_T for the different quark flavors using spin correlations would be one of the goals of the analyses proposed in the current paper.

The above heavy-quark argument does not apply to the s quark, but LEP experiments have shown that Λ baryons from s quarks still preserve a large fraction of the polarization [28–30].

Describing the polarization transfer from a quark to a baryon in terms of two numbers, r_L and r_T , is an approximation. More generally, the polarization transfer will depend on the fraction of the jet momentum carried by the baryon,

$$z = \frac{p_T^{\Lambda_q}}{p_T^{\text{jet}}}, \quad (2.2)$$

and is described by the so-called *spin-dependent* (or *polarized*) *fragmentation functions* [34, 35, 39, 40]. These functions vary slowly as a function of the energy scale of the process due to the renormalization group evolution [39, 40]. Characterizing these effects and taking them into account will require high-statistics measurements that could follow up the measurements motivated here and in refs. [18, 19, 21]. The only case where it is absolutely essential to take the z dependence into account is that of the strange quark. Due to their low mass, soft strange quarks are copiously produced in parton showering. To reduce these contributions, it is essential to focus on Λ baryons with high values of z . The dependence of the Λ polarization on z has been measured in Z decays at LEP [28–30] confirming the expectation [41] that the polarization of the initial strange quark is preserved primarily in high- z Λ baryons. For example, as has been estimated in ref. [19] based on the LEP measurements, roughly 60% of the strange-quark polarization is preserved in Λ baryons with $z > 0.3$. Additional information can be obtained using $t\bar{t}$ samples at the LHC [19].

3 Baryon Production and Relevant Decay Channels

The fragmentation fractions for producing the baryons of interest at high energies are shown in table 1. While the numbers for $b \rightarrow \Lambda_b$ and $c \rightarrow \Lambda_c$ are available in the literature, for the Λ we obtained the number from a Pythia [47] simulation. The simulation results are shown in figure 1, which presents the integrated fragmentation functions

$$f(s \rightarrow \Lambda, z > z_0) = \int_{z_0}^1 f_{s \rightarrow \Lambda}(z) dz \quad (3.1)$$

Fragmentation Fraction		Decay Scheme	BR	Spin analyzing power
$b \rightarrow \Lambda_b$	7.0% [18]	$\Lambda_b \rightarrow X_c \mu^- \bar{\nu}_\mu$	11% [42]	$\alpha_{\mu^-} \approx -0.26$, $\alpha_{\bar{\nu}_\mu} \approx 1$ [18, 43]
		with $\Lambda \rightarrow p\pi^-$	2.7% [42]	
		with Λ_c^+ reco.	2.0% [42]	
$c \rightarrow \Lambda_c$	6.4% [44]	$\Lambda_c^+ \rightarrow pK^-\pi^+$	6.3% [42]	$\alpha_{\text{eff}} \approx 0.662$ [45]
		$\Lambda_c^+ \rightarrow \Lambda\mu^+\nu_\mu$	3.5% [42]	$\alpha_{\mu^+} \approx 1$ [46]
		with $\Lambda \rightarrow p\pi^-$	2.2% [42]	
$s \rightarrow \Lambda$ ($z > 0.3$)	2.8% [47, 48]	$\Lambda \rightarrow p\pi^-$	64% [42]	$\alpha_p \approx 0.75$ [42]

Table 1: Baryon fragmentation fractions, relevant decay schemes, branching ratios (BR) and spin analyzing powers (asymmetry parameters) of the decays.

and similarly for $s \rightarrow \bar{\Lambda}$. This gives the following fragmentation fractions for $z_0 = 0.3$ (a cut motivated at the end of section 2):

$$f(s \rightarrow \Lambda, z > 0.3) = 2.8\%, \quad f(s \rightarrow \bar{\Lambda}, z > 0.3) = 0.3\%. \quad (3.2)$$

We also compute the sum of the Λ and $\bar{\Lambda}$ numbers for a comparison with the AKKII data-based results [48]. A reasonable rough agreement is seen, except at the high- z tail where neither of the methods can be trusted.

Table 1 also shows the decay channels we consider, selected based on their branching ratio (BR), spin analyzing power, and feasibility of identification and reconstruction. For the semileptonic Λ_b decays, we consider three types of selections (similar to ref. [18]):

- *Inclusive Selection*, where X_c represents any collection of particles containing a charmed hadron, which is usually a Λ_c^+ .¹ This selection, which will not apply any conditions to the particles produced along with the muon, will have high signal efficiency, but also unsuppressed backgrounds from semileptonic decays of b mesons.
- *Semi-inclusive Selection*, where the X_c is required to contain a $\Lambda \rightarrow p\pi^-$ decay, to reduce backgrounds from the semileptonic b -meson decays.
- *Exclusive Selection*, where the X_c is required to contain a fully reconstructible Λ_c^+ decay (i.e., with charged products only), to reduce backgrounds from the semileptonic meson decays and facilitate the reconstruction of the Λ_b decay kinematics for the polarization and spin correlation measurements. The full list of the Λ_c^+ decays we include here is provided in a later section, in table 15.

In the semileptonic Λ_c^+ decay case, only the selection with the $\Lambda \rightarrow p\pi^-$ decay will be considered. Decays with electrons instead of muons, for both the Λ_b and Λ_c^+ , can be used

¹The branching ratios for Λ_b decays to charmed mesons are very small, e.g. $\text{BR}(\Lambda_b \rightarrow D^0 p \pi^-) \approx 6 \times 10^{-4}$, $\text{BR}(\Lambda_b \rightarrow D^{(*)+} p \pi^- \pi^-) \approx 8 \times 10^{-4}$ [42]. We will neglect them in the following.

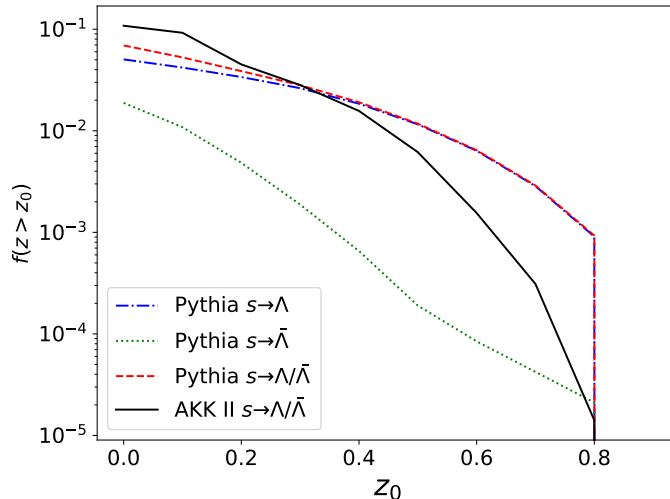


Figure 1: The fragmentation fraction for $z > z_0$, for $s \rightarrow \Lambda$, $s \rightarrow \bar{\Lambda}$, and $s \rightarrow \Lambda/\bar{\Lambda}$, where $\Lambda/\bar{\Lambda}$ denotes that either a Λ or $\bar{\Lambda}$ is produced in the s -quark hadronization. The Pythia simulation was run at $\sqrt{s} = 14$ TeV with $p_T > 400$ GeV and $|\eta| < 2.5$ cuts on the jets, which were clustered with the anti- k_t jet algorithm with radius $R = 0.4$ [52, 53] and matched to the parton-level s quarks. We also show the data-based AKKII results [48].

as well. Their branching ratios and spin analyzing powers are approximately the same as for the decays with muons, and the trigger thresholds for electrons and muons are comparable. However, we will conservatively not take decays with electrons into account since reconstruction of electrons inside jets usually has low efficiency or high background [49–51].

The last column in table 1 indicates the decay products whose angular distributions are intended to be used for the polarization and spin correlation measurements. The spin analyzing power (or the asymmetry parameter) α is defined by writing the angular distribution of the decay as

$$\frac{1}{\Gamma} \frac{d\Gamma}{d \cos \theta} = \frac{1}{2} (1 + \alpha \mathcal{P} \cos \theta), \quad (3.3)$$

where θ is the angle between the momentum of the decay product and the direction of the baryon polarization $\vec{\mathcal{P}}$, in the baryon rest frame.² This provides a handle for measuring the baryon and antibaryon polarizations and spin correlations.

The $\Lambda_c^+ \rightarrow pK^-\pi^+$ decay can proceed via various intermediate resonances, with different angular distributions in each case, and we quote the effective value of the spin analyzing power, α_{eff} , that corresponds to the sensitivity that can be obtained with a full amplitude analysis [45].

Reconstructing the kinematics of the semileptonic decays, which is needed for the polarization and spin correlation measurements, is not straightforward because neutral

²To define α for the corresponding antibaryon decay, we will follow the common convention (as in refs. [1, 2, 8], for example, but unlike in ref. [15]) of adding a minus sign in front of the α in eq. (3.3) for the antibaryon, such that for CP conserving decays α has the same value for the baryon and antibaryon decay.

particles cannot be assigned to a vertex and neutrinos are not observed at all. However, it can be done with certain approximations using the method described in detail in sections 4.2.2 and 4.2.3 of ref. [18], for example. It uses the fact that the energy fraction carried by a heavy-flavored hadron (relative to the original quark) has a relatively peaked distribution, with an average value around 70% for the b quark [54–60] and 50% for the c quark [61, 62].³ To reconstruct the neutrino momentum, the vector pointing from the primary vertex to the baryon decay vertex is taken as the baryon flight direction. See also refs. [64–67]. Unfolding will be required to account for the approximations made.

4 Polarization and Spin Correlations

We will now review the mathematical description of the polarization and spin correlations of $q\bar{q}$ pairs and describe how these properties are expected to manifest themselves in angular distributions of the baryon decays.

4.1 Quark-Antiquark Pair Spin State Description

The spin state of a quark and antiquark is described by a density matrix of the form [68]

$$\rho = \frac{1}{4} \left(\mathbb{1} \otimes \mathbb{1} + \tilde{B}_i^+ \sigma^i \otimes \mathbb{1} + \tilde{B}_i^- \mathbb{1} \otimes \sigma^i + \tilde{C}_{ij} \sigma^i \otimes \sigma^j \right). \quad (4.1)$$

Here $\mathbb{1}$ is a 2×2 unit matrix, σ^i are the Pauli matrices, the indices (summation over which is implied) represent the coordinate axes, $\tilde{\mathbf{B}}^\pm$ are three-dimensional vectors characterizing the polarization of the quark and antiquark,⁴ and $\tilde{\mathbf{C}}$ is a 3×3 matrix that characterizes the spin correlations between them. The tilde symbol is used here to distinguish between these properties of the quark and antiquark and the measurable coefficients of the related angular distributions that will be defined in the next subsection.

As common in the $t\bar{t}$ literature [8, 13, 15], we will use the orthogonal set of axes $\{\hat{k}, \hat{n}, \hat{r}\}$. The axis \hat{k} is defined as the direction of the outgoing quark’s momentum in the partonic center-of-mass (CM) frame. To define the other axes, we denote by \hat{p} the momentum direction of one of the incoming partons, and by Θ the scattering angle of the outgoing quark, such that $\cos \Theta = \hat{k} \cdot \hat{p}$. Then the axes \hat{n} and \hat{r} are defined as

$$\hat{n} = \text{sign}(\cos \Theta) \frac{\hat{p} \times \hat{k}}{\sin \Theta}, \quad \hat{r} = \text{sign}(\cos \Theta) \frac{\hat{p} - \hat{k} \cos \Theta}{\sin \Theta}. \quad (4.2)$$

The $\text{sign}(\cos \Theta)$ factor is included in eq. (4.2) to account for the Bose symmetry of the gg initial state, meaning that without this sign factor the gg -initiated contributions to the polarizations and spin correlations of the sample as a whole will cancel between events with $\cos \Theta < 0$ and $\cos \Theta > 0$, as can also be seen explicitly in refs. [69, 70]. It is of note that the inclusion of the $\text{sign}(\cos \Theta)$ factor leads to partial cancellation for events originating from $q\bar{q}$ [69, 70]. It can be useful to also do a measurement without this factor to be more sensitive

³These numbers are appropriate for quark p_T values of tens of GeV. They decrease slowly as a function of the energy scale due to renormalization group evolution [63].

⁴The quark polarization is $\tilde{\mathbf{B}}^+$, and the antiquark polarization is $-\tilde{\mathbf{B}}^-$.

to $q\bar{q}$ -initiated contributions. CMS measured the Λ_b polarization along the \hat{n} axis without the sign factor, using an amplitude analysis of the decay⁵ $\Lambda_b \rightarrow J/\psi(\rightarrow \mu^+\mu^-)\Lambda(\rightarrow p\pi^-)$ at CM energies $\sqrt{s} = 7$ and 8 TeV, finding $\mathcal{P} = 0.00 \pm 0.06$ (stat.) ± 0.06 (syst.) [33]. LHCb conducted Λ_b polarization measurements using the same decay channel and found the polarization along \hat{n} (without the sign factor) to be within 68% credibility level intervals of $[-0.06, 0.05]$, $[-0.04, 0.05]$ and $[-0.01, 0.07]$ at $\sqrt{s} = 7, 8$ and 13 TeV, respectively [32]. The absence of the sign factor in the LHCb measurement does not lead to a cancellation of the gg -initiated contributions since the LHCb detectors have coverage only in the forward direction.

Given the orthonormal basis $\{\hat{k}, \hat{n}, \hat{r}\}$, we can write the polarization vectors and spin correlation matrix as

$$\tilde{\mathbf{B}}^\pm = b_k^\pm \hat{k} + b_n^\pm \hat{n} + b_r^\pm \hat{r} \quad (4.3)$$

and

$$\begin{aligned} \tilde{\mathbf{C}} &= c_{kk} \hat{k}\hat{k} + c_{nn} \hat{n}\hat{n} + c_{rr} \hat{r}\hat{r} \\ &+ c_{rk}(\hat{r}\hat{k} + \hat{k}\hat{r}) + c_{nr}(\hat{n}\hat{r} + \hat{r}\hat{n}) + c_{kn}(\hat{k}\hat{n} + \hat{n}\hat{k}) \\ &+ c_n(\hat{r}\hat{k} - \hat{k}\hat{r}) + c_k(\hat{n}\hat{r} - \hat{r}\hat{n}) + c_r(\hat{k}\hat{n} - \hat{n}\hat{k}) \end{aligned} \quad (4.4)$$

or equivalently

$$\tilde{\mathbf{C}} = \begin{pmatrix} c_{kk} & c_{kn} + c_r & c_{rk} - c_n \\ c_{kn} - c_r & c_{nn} & c_{nr} + c_k \\ c_{rk} + c_n & c_{nr} - c_k & c_{rr} \end{pmatrix}. \quad (4.5)$$

In this way of writing, the symmetric part of the matrix $\tilde{\mathbf{C}}$ is described by the components

$$c_{ij} = \frac{1}{2} (\tilde{C}_{ij} + \tilde{C}_{ji}) \quad (4.6)$$

and the antisymmetric part by

$$c_\ell = \frac{1}{2} \epsilon_{ij\ell} \tilde{C}_{ij}. \quad (4.7)$$

The range of possible values for b_i^\pm , c_{ij} , and c_ℓ is $[-1, 1]$. These quantities in general depend on the production process, the partonic CM energy squared \hat{s} , and the quark's scattering angle Θ in relation to the proton going in the positive direction of the \hat{z} axis.

Table 2 classifies the polarization and spin correlation components according to their P and CP properties. The P and CP invariance of QCD (neglecting θ_{QCD}) allows spin correlations only in c_{kk} , c_{rr} , c_{nn} , and c_{rk} . For the polarizations, nonzero $b_n^+ = b_n^-$ are allowed, but expected to be small as these polarizations only appear at NLO QCD and are proportional to the quark mass [69, 70]. Small contributions involving the electroweak interactions are expected in many of the components (see, e.g., ref. [8], where they were computed for the top quark), but we will not consider them in this paper.

⁵The advantage of this decay chain is that every product is charged and therefore has a track, so one can reconstruct it exactly, leading to low backgrounds and precise kinematics. The downside of this channel is its tiny branching ratio ($\sim 3 \times 10^{-5}$).

Component	P	CP
$b_k^+ + b_k^-$	Odd	Even
$b_k^+ - b_k^-$	Odd	Odd
$b_r^+ + b_r^-$	Odd	Even
$b_r^+ - b_r^-$	Odd	Odd
$b_n^+ + b_n^-$	Even	Even
$b_n^+ - b_n^-$	Even	Odd
c_{kk}	Even	Even
c_{rr}	Even	Even
c_{nn}	Even	Even
c_{rk}	Even	Even
c_n	Even	Odd
c_{nr}	Odd	Even
c_k	Odd	Odd
c_{kn}	Odd	Even
c_r	Odd	Odd

Table 2: P and CP properties of the polarization and spin correlation components.

4.2 Decay Angular Distributions

Similar to the $t\bar{t}$ case [8], if we denote the momentum vector of one of the baryon decay products in the baryon rest frame by \mathbf{p}_1 , and the momentum vector of one of the antibaryon decay products in the antibaryon rest frame by \mathbf{p}_2 , their angular distributions are given by

$$\frac{1}{\sigma} \frac{d\sigma}{d\Omega_1 d\Omega_2} = \frac{1}{(4\pi)^2} (1 + \mathbf{B}^+ \cdot \hat{\mathbf{p}}_1 + \mathbf{B}^- \cdot \hat{\mathbf{p}}_2 - \hat{\mathbf{p}}_1 \cdot \mathbf{C} \cdot \hat{\mathbf{p}}_2), \quad (4.8)$$

where

$$B_i^\pm = \alpha_\pm r_i f \tilde{B}_i^\pm, \quad C_{ij} = \alpha_+ \alpha_- r_i r_j f \tilde{C}_{ij}. \quad (4.9)$$

Here $\tilde{\mathbf{B}}^\pm$ and $\tilde{\mathbf{C}}$ are the quark and antiquark polarization vectors and their spin correlation matrix from eqs. (4.3)–(4.4). The factors α_+ and α_- , referring to the baryon and antibaryon, respectively, are the spin analyzing powers of their decays, as defined in eq. (3.3). The factors r_i are the polarization retention factors from eq. (2.1): r_L for the \hat{k} axis and r_T for the \hat{n} and \hat{r} axes.⁶ The factor f is the sample purity, namely the fraction of signal events out of the total number of selected events:

$$f = \frac{N_{\text{sig}}}{N_{\text{bg}} + N_{\text{sig}}}. \quad (4.10)$$

⁶We work here in the approximation that the baryon momentum is parallel to the quark momentum and the only effect is the scaling of the polarization by the corresponding factor.

The multiplication by f in eq. (4.9) is only correct if we assume that the effect of the background is only to dilute the B^\pm and C coefficients. This would be the case, for example, for a background consisting of unpolarized and uncorrelated baryon-antibaryon pairs. If the background has a more general angular dependence, it will add a bias that will need to be subtracted. In some cases it will be possible to measure the bias using sidebands; in other cases it can be estimated through simulation.

It will also be useful for us to define

$$C_{ij}^\pm = C_{ij} \pm C_{ji} \quad (4.11)$$

and rewrite eq. (4.9) as

$$B_i^\pm = \alpha_\pm r_i f b_i^\pm, \quad C_{ii} = \alpha_+ \alpha_- r_i^2 f c_{ii}, \quad C_{ij}^+ = 2\alpha_+ \alpha_- r_i r_j f c_{ij}, \quad C_{ij}^- = 2\alpha_+ \alpha_- r_i r_j f c_\ell, \quad (4.12)$$

where we used eqs. (4.6)–(4.7). In the expression for C_{ij}^- , the axes corresponding to the indices i , j and ℓ are related via $\hat{i} \times \hat{j} = \hat{\ell}$.

Defining sets of spherical coordinates around the axes of interest for the baryon and antibaryon and integrating eq. (4.8) over the azimuthal angles gives

$$\frac{1}{\sigma} \frac{d\sigma}{d \cos \theta_i^+ d \cos \theta_j^-} = \frac{1}{4} \left(1 + B_i^+ \cos \theta_i^+ + B_j^- \cos \theta_j^- - C_{ij} \cos \theta_i^+ \cos \theta_j^- \right), \quad (4.13)$$

where θ_i^+ (θ_j^-) is the angle between the direction of the decay product and the chosen axis, in the baryon (antibaryon) rest frame.⁷ Integrating over one of the θ s in eq. (4.13), we get the distributions

$$\frac{1}{\sigma} \frac{d\sigma}{d \cos \theta_i^\pm} = \frac{1}{2} \left(1 + B_i^\pm \cos \theta_i^\pm \right), \quad (4.14)$$

through which one can measure B_i^\pm to obtain the quark and antiquark polarization components b_i^\pm . Converting the double differential distribution in eq. (4.13) to a distribution differential in the product $\cos \theta_i^+ \cos \theta_j^-$, we obtain

$$\frac{1}{\sigma} \frac{d\sigma}{d(\cos \theta_i^+ \cos \theta_j^-)} = \frac{1}{2} \left(1 - C_{ij} \cos \theta_i^+ \cos \theta_j^- \right) \ln \left(\frac{1}{|\cos \theta_i^+ \cos \theta_j^-|} \right), \quad (4.15)$$

through which one can measure the C_{ij} prefactors related to the spin correlations. We imagine using them to extract the diagonal (c_{ii}) components of the spin correlation matrix. For the off-diagonal components, which are useful to divide into symmetric (c_{ij}) and antisymmetric (c_ℓ) parts because of their different CP properties (recall table 2), one can derive from eq. (4.8) the distribution

$$\frac{1}{\sigma} \frac{d\sigma}{dX_\pm} = \frac{1}{2} \left(1 - \frac{C_{ij}^\pm}{2} X_\pm \right) \cos^{-1}(|X_\pm|), \quad (4.16)$$

where $X_\pm = \cos \theta_i^+ \cos \theta_j^- \pm \cos \theta_j^+ \cos \theta_i^-$. The components c_{ij} (with $i \neq j$) and c_ℓ can be computed from C_{ij}^\pm via eq. (4.12).

⁷For the antibaryon, we take the reference axes to be opposite to the $\{\hat{k}, \hat{n}, \hat{r}\}$ axes defined for the baryon, following the convention of ref. [8]. In combination with the convention described in footnote 2, this makes our signs for B_i^\pm and C_{ij} agree with both ref. [8] and ref. [15].

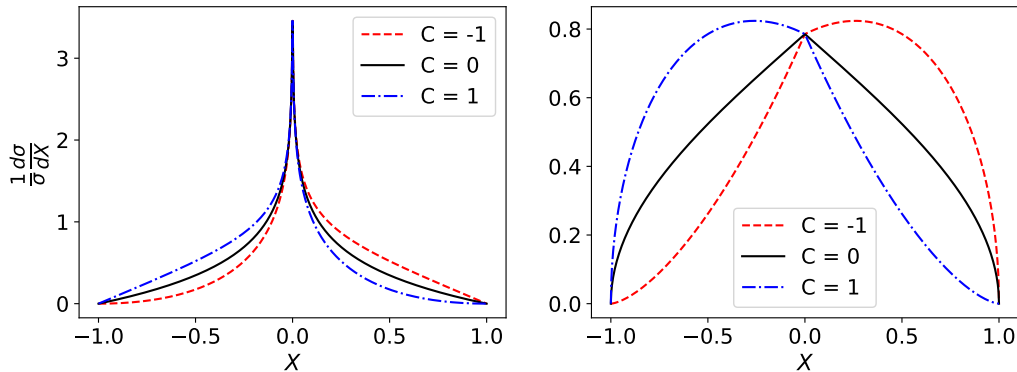


Figure 2: Distributions of $X = \cos \theta_i^+ \cos \theta_i^-$ (left) and $X = \cos \theta_i^+ \cos \theta_j^- \pm \cos \theta_j^+ \cos \theta_i^-$ (right), from which the spin correlations can be extracted. The distributions are based on eqs. (4.15)–(4.16), and are shown for three different values of the coefficient C_{ii} (left) and $C_{ij}^\pm/2$ (right).

The distributions in eq. (4.14) are straight lines, while the shapes of the distributions in eqs. (4.15) and (4.16) are shown in figure 2. They are plotted for C_{ii} and $C_{ij}^\pm/2$ values of ± 1 (which are the upper and lower bounds) and 0.

4.3 Statistical Uncertainty Evaluation

The statistical uncertainty of the coefficients B_i^\pm , C_{ij} , and C_{ij}^\pm , when they are extracted from fits of data to eqs. (4.14), (4.15), and (4.16), respectively, is given approximately by

$$\Delta B_i^\pm \simeq \frac{\sqrt{3}}{\sqrt{N}}, \quad \Delta C_{ij} \simeq \frac{3}{\sqrt{N}}, \quad \Delta C_{ij}^\pm \simeq \frac{3\sqrt{2}}{\sqrt{N}}, \quad (4.17)$$

where N is the number of events. These results are derived in appendix A. Using eq. (4.12) we then obtain for the statistical uncertainties of the polarization and spin correlation components

$$\Delta b_i^\pm \simeq \frac{\sqrt{3}}{|r_i \alpha_\pm| \sqrt{f N_{\text{sig}}}}, \quad (4.18)$$

$$\Delta c_{ii} \simeq \frac{3}{r_i^2 |\alpha_+ \alpha_-| \sqrt{f N_{\text{sig}}}}, \quad (4.19)$$

$$\Delta c_{ij(\ell)} \simeq \frac{3}{\sqrt{2} |r_i r_j \alpha_+ \alpha_-| \sqrt{f N_{\text{sig}}}}, \quad (4.20)$$

where N_{sig} is the number of signal events, and the notation $c_{ij(\ell)}$ means to refer at once to c_{ij} from eq. (4.6) and c_ℓ from eq. (4.7). The uncertainty in eq. (4.18) applies to b_i^+ and b_i^- separately. The quantities with definite P and CP properties formed from the sums and differences of b_i^+ and b_i^- (recall table 2) will have lower relative statistical uncertainties since both the quark and antiquark measurements will contribute.

We note that these formulas only provide rough estimates of the expected statistical uncertainties, mainly because they do not take into account effects of unfolding or nontrivial angular distributions of the background.

5 Quark Polarization and Spin Correlations in QCD

We used MadGraph [71] to obtain the leading-order (LO) QCD expectations for the polarization and spin correlations in $pp \rightarrow b\bar{b}$ and $pp \rightarrow c\bar{c}$.

We first validated our procedure on the process $pp \rightarrow t\bar{t}$, results for which are available in the literature [11]. As a technical tool, we decayed the top quark as $t \rightarrow b\ell^+\nu_\ell$ with MadSpin [72] (and similarly for \bar{t}) to obtain the polarization and spin correlation information of the t and \bar{t} from the angular distributions of the leptons. We used the NN23LO1 parton distribution functions and the default dynamical factorization and renormalization scales defined in MadGraph. The simulation was inclusive, with no cuts applied, as relevant for the comparison with the numbers in ref. [11]. As a check, we have also run the full matrix element simulation in MadGraph, namely $pp \rightarrow b\ell^+\nu_\ell\bar{b}\ell^-\bar{\nu}_\ell$ without separating the process into production and decay, and obtained consistent results.

The symmetries of LO QCD dictate that only the components c_{kk} , c_{rr} , c_{nn} , and c_{rk} can be nonzero [8]. We indeed find all the other components to be consistent with zero. For the non-vanishing components, we found good agreement with the LO results of ref. [11].

To obtain the polarizations and spin correlations for $pp \rightarrow b\bar{b}$ and $pp \rightarrow c\bar{c}$, we cannot follow a procedure exactly analogous to what we did for $pp \rightarrow t\bar{t}$ since MadGraph does not allow decaying b and c quarks (which we need as a technical tool to extract the spin information of the quarks). Instead, relying on the flavor blindness of QCD, we simulated $pp \rightarrow t\bar{t}$ with the top-quark mass set to m_b or m_c (and its width set to a negligible value). We have also lowered the masses of the particles that participate in the top decay $t \rightarrow b\ell^+\nu_\ell$, so that the decay will still happen. We have verified, by simulating the decay of a polarized top quark in this model using the method of ref. [73], that the spin analyzing power of the lepton remains the same.

Unlike in the $t\bar{t}$ case, where an inclusive measurement without any cuts on the t and \bar{t} is possible (with the use of unfolding), a measurement in $b\bar{b}$ or $c\bar{c}$ will typically be limited by triggers. (Triggers will be discussed in detail in section 6.1.) As we will see in later sections, the muon-based triggers are the best for our purposes. Since we work in MadGraph, at the level of parton-level quarks, instead of applying cuts on the muons produced in the hadron decays, we will apply roughly equivalent cuts on the quarks. Using a Pythia simulation, we found that applying the Run 2 ATLAS dimuon trigger threshold to muons from $b \rightarrow c$ transitions in the $b\bar{b}$ case is equivalent in terms of the cross section to applying the cuts $|\eta| < 2.4$ and $p_T > 79$ GeV on the quarks (“jets”). In the $c\bar{c}$ case the same procedure leads to a $p_T > 115$ GeV cut on the quarks.⁸ We will use these cuts here as an example.

The results for the non-vanishing spin correlation components are shown in table 3. We also present the inclusive values for a more meaningful comparison with the $t\bar{t}$ case, as a check. For the inclusive $b\bar{b}$ and $c\bar{c}$ simulations we fixed the factorization and renormalization scales to 10 GeV, to avoid large artifacts from low energies. As can be seen in the table, the inclusive values are rather similar between $t\bar{t}$, $b\bar{b}$, and $c\bar{c}$. The cuts, on the other hand, take

⁸The difference between $b\bar{b}$ and $c\bar{c}$ is mostly related to the fact that a b hadron typically carries around 70% of the b -jet momentum, while a c hadron carries around 50% of the c -jet momentum, so c quarks need to be more energetic for their muons to pass the trigger threshold.

	$t\bar{t}$, no cuts	$b\bar{b}$, no cuts	$c\bar{c}$, no cuts	$b\bar{b}$ with cuts	$c\bar{c}$ with cuts
c_{kk}	0.324 ± 0.006	0.296 ± 0.004	0.284 ± 0.004	-0.987 ± 0.004	-0.984 ± 0.006
c_{rr}	0.009 ± 0.006	0.004 ± 0.004	-0.006 ± 0.004	-0.603 ± 0.004	-0.609 ± 0.006
c_{nn}	0.333 ± 0.006	0.299 ± 0.004	0.298 ± 0.004	0.591 ± 0.004	0.603 ± 0.006
$2c_{rk}$	-0.211 ± 0.008	-0.197 ± 0.006	-0.188 ± 0.006	-0.038 ± 0.006	-0.008 ± 0.009

Table 3: Spin correlations in $b\bar{b}$ and $c\bar{c}$ events with and without cuts for Run 2 ($\sqrt{s} = 13$ TeV). For comparison, we also show the same quantities for the $t\bar{t}$ case. The uncertainties shown are the statistical uncertainties of our simulation.

	$b\bar{b}$, no cuts	$c\bar{c}$, no cuts	$b\bar{b}$ with cuts	$c\bar{c}$ with cuts
c_{kk}	0.298 ± 0.004	0.276 ± 0.004	-0.972 ± 0.004	-0.995 ± 0.006
c_{rr}	-0.001 ± 0.004	-0.009 ± 0.004	-0.587 ± 0.004	-0.610 ± 0.006
c_{nn}	0.302 ± 0.004	0.284 ± 0.004	0.577 ± 0.004	0.596 ± 0.006
$2c_{rk}$	-0.187 ± 0.006	-0.188 ± 0.006	-0.054 ± 0.006	-0.015 ± 0.009

Table 4: Spin correlations in $b\bar{b}$ and $c\bar{c}$ events with and without cuts for the HL-LHC with $\sqrt{s} = 14$ TeV. The uncertainties shown are the statistical uncertainties of our simulation.

us to a completely different regime. This is understandable since the inclusive contributions are dominated by a region near the production threshold while the cuts select regions away from the threshold.

Table 4 presents the analogous results for the HL-LHC with $\sqrt{s} = 14$ TeV, where our effective cuts on the quarks are $|\eta| < 2.5$ and $p_T > 59$ GeV for $b\bar{b}$ and $p_T > 80$ GeV for $c\bar{c}$. We can see similar effects from the cuts as in the Run 2 case.

To assess systematic uncertainties, we examined the effects of varying the renormalization and factorization scales up and down by a factor of 2. While there was a significant effect on the cross sections, there were no significant effects on the spin correlation coefficients relative to the statistical uncertainties of our simulations, which are shown in tables 3 and 4.

6 Proposed Analyses and Their Prospects

In this section we will consider a variety of analysis channels for measuring the polarizations or spin correlations in $pp \rightarrow q\bar{q}$ processes with $q = s, c, \text{ or } b$, using the baryon decays that were listed in table 1.

We will need to address a variety of backgrounds. There are *intrinsic backgrounds*, which arise from the same parton-level process as the signal but with a different hadron decay passing the selection. There are also *extrinsic backgrounds*, which arise due to other parton-level processes that may involve the same baryon decay as the signal or another similar hadron decay. Lastly, there are *combinatorial backgrounds* (which may be of an

	ATLAS		CMS	
	Run 2	HL-LHC	Run 2	HL-LHC
Collider energy \sqrt{s} [TeV]	13	14	13	14
Integrated luminosity \mathcal{L} [fb^{-1}]	140	3000	140	3000
Jet p_T cut [GeV]	460	400	500	520
Double muon p_T cut (without isolation) [GeV]	15	10	37, 27	37, 27
Single muon p_T cut (with isolation) [GeV]	27	20	24	24
Double electron p_T cut (without isolation) [GeV]	18	10	25	25
Single electron p_T cut (with isolation) [GeV]	27	22	28	32 or 26
Jet $ \eta $ cut	2.4	3.8	2.4	4.0
Muon $ \eta $ cut	2.4	2.5	2.4	2.4
Electron $ \eta $ cut	2.4	2.5	2.4	2.4

Table 5: The collider energy, luminosity, and trigger-motivated cuts for Run 2 of the LHC and those that are planned for the HL-LHC in ATLAS [74] and CMS [75]. We will be using the ATLAS cuts.

intrinsic or extrinsic origin), which are a result of random tracks forming by chance a vertex similar to that of the baryon decay of interest. While the probability of this happening will usually be low, such a background can still be significant if the total cross section of the corresponding process is large.

We will assess the feasibility of each channel in terms of the precision that can be achieved and the sample purity. We will do it with the help of MadGraph [71] and/or Pythia [47] simulations and reliance on elements of existing ATLAS and CMS analyses. For jet clustering, the Pythia simulations are interfaced with FastJet [53], where we use the anti- k_t algorithm with radius $R = 0.4$ [52]. Apart from trigger-motivated cuts and background reduction cuts relevant in each case, we will present our results for several values of dijet invariant mass (m_{jj}) cuts (in cases where statistics allows that) since such a selection can enhance the sensitivity to BSM effects that become sizable only at high energies.

We will start by presenting our assumed datasets, based on the current and future planned LHC parameters and triggers, and then proceed to discussing the individual analysis channels, each with its own backgrounds and selection strategy.

6.1 Benchmark Datasets

We will consider the currently available full Run 2 dataset as well as the HL-LHC dataset. Table 5 presents the main parameters defining these datasets, including the standard trigger-motivated cuts that we will be assuming. The numbers shown in the table are for the offline cuts from ATLAS [74] and the online ones for CMS [75]. We will be using the ATLAS cuts.

For the jet based triggers, which are relevant for the hadronic channels $c \rightarrow \Lambda_c^+ \rightarrow pK^-\pi^+$ and $s \rightarrow \Lambda \rightarrow p\pi^-$, for Run 2 we added the requirement $|\eta| < 2.4$ (even though the trigger functions up to $|\eta| = 2.8$ [76]) so that the jets will be within the tracker. For the HL-LHC we require $|\eta| < 3.8$.

For the semileptonic channels $b \rightarrow \Lambda_b \rightarrow X_c\mu^-\bar{\nu}_\mu$ and $c \rightarrow \Lambda_c^+ \rightarrow \Lambda\mu^+\nu_\mu$ we can use the muon triggers, whose thresholds are much softer than those of the jet triggers. Even though the muon carries only a fraction of the jet energy, the muon triggers will still provide higher statistics. Since our muons are inside jets, the triggers of interest are primarily those that do not require the muons to be isolated. That is not a problem for events with two muons since double muon triggers without isolation requirements have sufficiently low thresholds. However, in some of the analyses that we will describe (semileptonic Λ_c^+ decay on one side and hadronic on the other side, or polarization measurements without any requirement on the second jet) just a single muon will be present. Single muon triggers without isolation have the relatively high thresholds of 50 GeV [75, 77]. We will instead be relying on the ATLAS single muon trigger (included in table 5) with a loose isolation criterion, which has around 50% efficiency for muons in heavy-flavor jets [77].

As was mentioned in section 3, decays with electrons instead of muons can be considered as well (even though reconstruction of electrons inside jets usually has low efficiency or high background), and table 5 shows the corresponding triggers.

In the context of the $b \rightarrow \Lambda_b \rightarrow X_c\mu^-\bar{\nu}_\mu$ channel, we also looked at b -tagging triggers. In ATLAS, the single b -jet trigger [78] requires $E_T > 225$ GeV (which is expected to become $p_T > 180$ GeV at the HL-LHC [74]), and the double b -jet trigger demands $E_T > 150$ GeV for the leading jet $E_T > 50$ GeV for the subleading one. Similarly, CMS is expected to have a double b -jet trigger with a $p_T > 128$ GeV cut at the HL-LHC [75]. Even though these thresholds are significantly lower than those of the generic jet triggers, we have checked that the much lower thresholds of the muon-based triggers still result in more statistics. This happens in our particular case because the b jets we are interested in always contain a muon. The b -jet triggers can however be useful at high invariant masses, where they can recover much of the efficiency loss due to the loose isolation requirement of the low- p_T single-muon triggers.

In addition to the standard trigger paths listed in table 5, we will consider the CMS “parked” b -hadron dataset that was collected during part of Run 2 using the *data parking* strategy with a single displaced muon trigger [36, 37]. The muon p_T threshold varied between 7 and 12 GeV depending on the luminosity, its track was required to be within $|\eta| < 1.5$, and satisfy a requirement on impact parameter significance. Despite the lower integrated luminosity of this dataset ($\sim 50 \text{ fb}^{-1}$) and the η restriction, the soft p_T threshold allowed collecting more statistics than the standard Run 2 muon triggers.

6.2 Analyses of $pp \rightarrow s\bar{s}$

For measuring the polarization and spin correlations in $pp \rightarrow s\bar{s}$, we consider events with $s \rightarrow \Lambda$ and $\Lambda \rightarrow p\pi^-$.

6.2.1 Λ Reconstruction, Efficiency and Signal Yield

The decay $\Lambda \rightarrow p\pi^-$ has a very distinct signature of a highly displaced vertex with a pair of oppositely charged tracks that reconstruct the Λ mass if they are assigned the proton and charged pion masses. The other similar decay, $K_S \rightarrow \pi^+\pi^-$, will usually fail the Λ mass reconstruction, and moreover can be vetoed without significant loss of signal efficiency by requiring that the two tracks do not reconstruct the K_S mass when assigned the charged pion masses. These Λ decays were reconstructed in multiple analyses in ATLAS (e.g., [79–82]) and CMS (e.g., [33, 83–86]).

There is, however, an important obstacle to reconstructing the decays of energetic Λ baryons. With increasing p_T they quickly become too displaced to be successfully reconstructed within the volume of the tracker. This can result in a very significant efficiency loss. To optimize the reconstruction efficiency of highly displaced tracks, ATLAS have developed the Large Radius Tracking (LRT) algorithm [87–89]. It has been used in multiple searches for long-lived BSM particles [90–97]. The LRT algorithm looks at hits remaining after the standard reconstruction, and tries to reconstruct the remaining tracks with looser conditions on the transverse and longitudinal impact parameters. The addition of this algorithm allows keeping decent track reconstruction efficiency up to decay radii d_T of about $d_T^{\text{max}} \approx 300$ mm, with the mean reconstruction efficiency up to this decay radius being roughly $\epsilon_{\text{track}} \approx 65\%$. It is of note that LRT was applied to only about 10% of the events in Run 2, but is going to be used regularly in Run 3 and at the HL-LHC after the LRT processing time was significantly improved [89]. Moreover, with the ATLAS tracker upgrade planned for the HL-LHC, it will be possible to address even larger decay radii, with average reconstruction efficiency of roughly $\epsilon_{\text{track}} \approx 80\%$ up to $d_T^{\text{max}} \approx 400$ mm [98]. We will be using the efficiency numbers with the LRT algorithm to estimate the Λ reconstruction efficiency, after accounting for the probability for the Λ to decay within the ranges mentioned above.

The average Λ decay radius in $pp \rightarrow s\bar{s}$ events can be estimated as

$$\langle d_T \rangle = \langle \gamma\beta_T \rangle c\tau = \frac{\langle p_{T,\Lambda} \rangle c\tau}{m_\Lambda} = \frac{\langle z p_{T,\text{jet}} \rangle c\tau}{m_\Lambda}, \quad (6.1)$$

where $c\tau \approx 7.9$ cm is the Λ lifetime and z is the Λ momentum fraction from eq. (2.2). Since the cross section decreases fast as a function of $p_{T,\text{jet}}$ and z , we can obtain rough estimates for $\langle d_T \rangle$ by taking $p_{T,\text{jet}}$ to be the trigger-motivated jet p_T threshold from table 5, and $z = 0.3$, which is the lowest value of z we will be willing to use since much softer Λ baryons are not correlated with the original strange-quark polarization, as was discussed in section 2. This gives $\langle d_T \rangle \sim 9.8$ m for Run 2 and 8.5 m for the HL-LHC. Since $\langle d_T \rangle \gg d_T^{\text{max}}$, the probability for the Λ to decay sufficiently early is $\epsilon_{d_T} \simeq d_T^{\text{max}}/\langle d_T \rangle \approx 3.1\%$ for Run 2 and 4.7% for the HL-LHC. More accurate numbers that we obtained from a Pythia simulation (which accounts for the full jet p_T and z distributions above their corresponding thresholds) are $\epsilon_{d_T} \approx 2.2\%$ for Run 2 and 3.4% for the HL-LHC. For background jets (which are a mixture of all $pp \rightarrow jj$ processes apart from $pp \rightarrow s\bar{s}$) the numbers are 2.4% and 3.7%, respectively.

Run 2			HL-LHC		
$\sigma_{s\bar{s}}$ [pb]	N_s	$N_{s\bar{s}}$	$\sigma_{s\bar{s}}$ [pb]	N_s	$N_{s\bar{s}}$
3.1	54	< 1	8.3	8.1×10^3	2

Table 6: Cross sections (with trigger-motivated cuts) and signal event counts (after the full selection) for measurements of s -quark polarization (N_s) and spin correlations ($N_{s\bar{s}}$).

The full reconstruction efficiency for the $\Lambda \rightarrow p\pi^-$ decay in signal jets is $\epsilon_\Lambda = \epsilon_{dT} \epsilon_{\text{track}}^2 \approx 0.93\%$ for Run 2 and 2.2% for the HL-LHC. For spin correlation measurements we need the efficiency for reconstructing both a Λ and a $\bar{\Lambda}$. Despite the correlation between the p_T of the two jets, we can still obtain a rough estimate by simply squaring the efficiency, $\epsilon_{\Lambda\bar{\Lambda}} \simeq \epsilon_\Lambda^2$, because the jet p_T values are distributed mainly near the threshold. This gives $\epsilon_{\Lambda\bar{\Lambda}} \approx 9 \times 10^{-5}$ for Run 2 and 5×10^{-4} for the HL-LHC.

Table 6 shows the numbers of expected signal events in Run 2 and at the HL-LHC. We show both the number of s jets available for the polarization measurement (N_s) and the number of $s\bar{s}$ pairs available for the spin correlation measurement ($N_{s\bar{s}}$) computed as

$$N_s = \mathcal{L} \sigma_{s\bar{s}} f(s \rightarrow \Lambda, z > 0.3) \text{BR}(\Lambda \rightarrow p\pi^-) \epsilon_\Lambda, \quad (6.2)$$

$$N_{s\bar{s}} = \mathcal{L} \sigma_{s\bar{s}} f^2(s \rightarrow \Lambda, z > 0.3) \text{BR}^2(\Lambda \rightarrow p\pi^-) \epsilon_{\Lambda\bar{\Lambda}}, \quad (6.3)$$

where the cross sections $\sigma_{s\bar{s}}$ (with the trigger-motivated cut on the jets) were computed in MadGraph. We see from table 6 that the number of events available for spin correlation measurements is going to be too low even at the HL-LHC. We will therefore proceed with investigating the prospects of polarization measurements only.

6.2.2 Background

The dominant background is due to Λ baryons produced in dijet processes other than $pp \rightarrow s\bar{s}$. While the number of Λ baryons produced in most of these processes falls with z faster than in the signal, their total cross section is large. As a result, their contribution ends up being significant.

Figure 3 shows the results of a Pythia simulation for the signal and backgrounds, where the backgrounds are split into three categories according to the produced partons: gg , qg , and qq (where q represents all flavors of quarks and antiquarks). The two leading jets in each event are considered as s jet candidates, except for $s\bar{s}$ events, where we matched the jets to partons to count only Λ baryons from s (but not \bar{s}) as signal. The numbers are presented as a function of z_0 , the cut on the momentum fraction z carried by the Λ . From these plots we can calculate the sample purity. For $z_0 = 0.3$, the purity is $f \approx 0.9\%$ for both Run 2 and the HL-LHC.

6.2.3 Measurement prospects

With the signal event counts and purities, we can use eq. (4.18) to compute the expected precision of the polarization measurements. We find the expected statistical uncertainty on

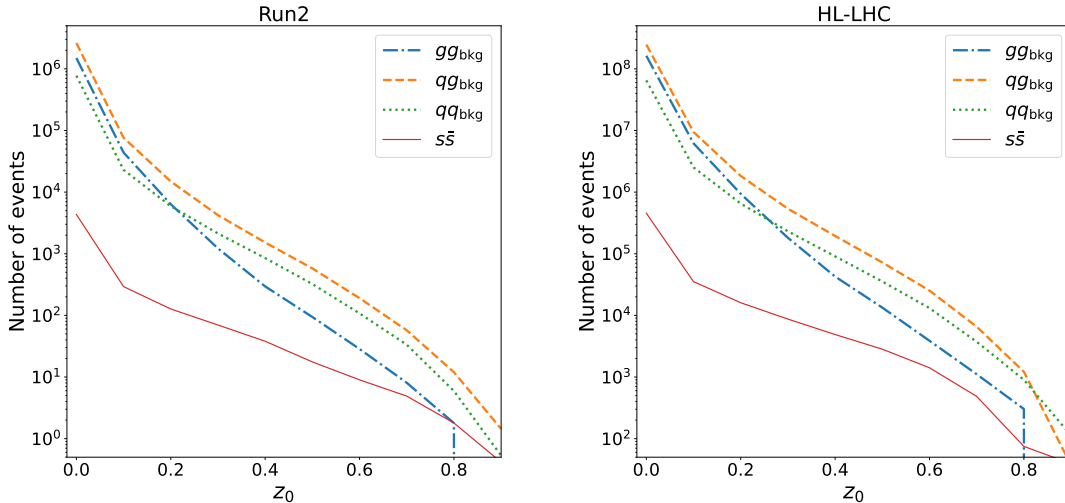


Figure 3: Expected number of events with reconstructed Λ baryons satisfying $z > z_0$ for the signal originating from $s\bar{s}$ events and backgrounds with the final state partons specified in the legend, for Run 2 (left) and the HL-LHC (right).

the polarization components b_i^\pm at the HL-LHC to be given by $r_i \Delta b_i^\pm \approx 0.27$. We show the result for the product $r_i \Delta b_i^\pm$ to provide numbers that are independent of the systematic uncertainty of the polarization retention factors r_i . We remind the reader, however, that $r_L \sim 0.6$, as mentioned in section 2. The physical range of b_i^\pm values is $[-1, 1]$. Only the HL-LHC results were discussed here since the Run 2 numbers are far from being promising.

We conclude that with the standard triggers we assumed, $s\bar{s}$ spin correlations cannot be measured, while polarization measurements might be possible at the HL-LHC, although the statistical uncertainty of the result is expected to be high, and the low purity of the sample will make the measurements difficult.

6.3 Analyses of $pp \rightarrow c\bar{c}$

For $c\bar{c}$ polarization and spin correlation measurements, we will consider in turn three possible analysis channels in terms of the Λ_c^+ decays: the *hadronic channel* where $\Lambda_c^+ \rightarrow pK^-\pi^+$, the *semileptonic channel* where $\Lambda_c^+ \rightarrow \Lambda\mu^+\nu_\mu$, and the *mixed channel* with the hadronic decay in one jet and the semileptonic decay in the other.

6.3.1 Hadronic Channel

The signature of the $\Lambda_c^+ \rightarrow pK^-\pi^+$ decay is one negatively and two positively charged tracks coming from a common vertex. They should also reconstruct the Λ_c^+ mass for an assignment of the proton and π^+ masses to the positively charged tracks and the K^- mass to the negatively charged one. Such decays were reconstructed by CMS in refs. [99, 100].

There are intrinsic backgrounds from various other decays of charmed hadrons, with examples shown in table 7. Some approaches for reducing them were discussed in ref. [18]. Extrinsic backgrounds from $pp \rightarrow b\bar{b}$ should be considered as well. They include Λ_c^+

Fragmentation Fraction [%]		Decay Scheme	Branching Ratio [%]
$c \rightarrow \Lambda_c^+$	6.4	$\Lambda_c^+ \rightarrow pK^-\pi^+$ (signal)	6.3
		$\Lambda_c^+ \rightarrow pK^-\pi^+\pi^0$	4.4
		$\Lambda_c^+ \rightarrow \Sigma^+\pi^-\pi^+$	4.5
		$\Lambda_c^+ \rightarrow \pi^+\pi^-\pi^+\Lambda$	3.6
$c \rightarrow D^+$	22.7	$D^+ \rightarrow \pi^+K^-\pi^+$	9.4
		$D^+ \rightarrow \pi^+K^-\pi^+\pi^0$	6.2
		$D^+ \rightarrow \pi^+\pi^-\pi^+K_S^0$	3.1
		$D^+ \rightarrow \pi^+\pi^-\pi^+\pi^0$	1.2
$c \rightarrow D^0$	61.8	$D^0 \rightarrow \pi^+K^-\pi^+\pi^-$	8.2
		$D^0 \rightarrow \pi^+K^-\pi^+\pi^-\pi^0$	4.3
$c \rightarrow D_s^+$	8.2	$D_s^+ \rightarrow K^+K^-\pi^+$	5.4
		$D_s^+ \rightarrow K^+K^-\pi^+\pi^0$	5.5
		$D_s^+ \rightarrow \pi^+K^-\pi^+K_S^0$	1.5

Table 7: The $\Lambda_c^+ \rightarrow pK^-\pi^+$ signal and some of its intrinsic backgrounds. The numbers are from refs. [42, 44]. The background decays will usually fail to reconstruct the Λ_c^+ mass—a requirement that will strongly suppress them.

baryons produced in Λ_b or B -meson decays as well as other decays that produce vertices that pass the selection. These contributions can be suppressed significantly using the large displacement of the b -hadron decays ($c\tau \approx 0.45$ mm) relative to the Λ_c^+ ($c\tau \approx 0.06$ mm). There is also the combinatorial background of three general tracks forming by chance a fake Λ_c^+ -like vertex.

Simulating the backgrounds for the $\Lambda_c^+ \rightarrow pK^-\pi^+$ decay with publicly available tools is nontrivial for us due to several reasons. First, the displacement of the Λ_c^+ vertex is small, so a careful simulation of the tracking resolution, as well as the vertexing algorithm, are needed to assess the impact of any displacement-related cuts. Second, simulating combinatorial background requires good control of tails of distributions of high cross section processes.

We can however get an idea about the size of the expected background and the signal efficiency from the CMS analysis in ref. [100]. CMS used several variables to select $\Lambda_c^+ \rightarrow pK^-\pi^+$ candidates: the χ^2 of the vertex fit to the three tracks, the angle between the Λ_c^+ candidate momentum and the vector connecting the production and decay vertices in the transverse plane, the transverse separation significance between the two vertices, and the Λ_c^+ p_T fractions carried by the kaon and by the proton. A distribution of the $pK^-\pi^+$ invariant mass was then constructed, with the Λ_c^+ contribution appearing as a narrow peak. The number of events in the peak is about 7.9% of the total number of events in the peak region for Λ_c^+ candidates with $20 < p_T < 30$ GeV. CMS estimate the prompt Λ_c^+ fraction in the peak to be between 0.79 to 0.88. We will therefore take our rough estimate for the

$c\bar{c}$, hadronic	Run 2				HL-LHC			
	m_{jj} cut [GeV]	$\sigma_{c\bar{c}}$ [pb]	N_c	$r_i\Delta b_i^\pm$	$N_{c\bar{c}}$	$\sigma_{c\bar{c}}$ [pb]	N_c	$r_i\Delta b_i^\pm$
no cut	3.0	420	0.48	< 1	8.0	2.4×10^4	0.045	24
1000	2.6	360			4.7	1.4×10^4	0.059	14
1500	0.57	80			0.93	2800	0.13	2
2000	0.13	18			0.21	650	0.28	

Table 8: Cross sections (with trigger-motivated cuts) and signal event counts (after the full selection) for measurements of c -quark polarization (N_c) and spin correlations ($N_{c\bar{c}}$) in the hadronic channel. The expected statistical uncertainties for the polarization measurements are shown as well. The sample purity is 6.9% for Run 2, and double that for the HL-LHC.

sample purity (when a single jet is considered) to be $f \approx 6.9\%$. CMS also report the signal efficiency to be roughly $\epsilon_{\Lambda_c^+} \approx 25\%$, which we will also assume. It should be noted that the invariant mass resolution will be improved by 20–50% at the HL-LHC [101–105] so the purity will improve accordingly. We shall be optimistic and reduce the background under the peak by a factor of two (i.e., approximately double the purity) in our estimates for the HL-LHC. We note that the upgraded tracking detectors will likely improve the efficacy of the other cuts used in the selection as well.

The sidebands of the $pK^-\pi^+$ invariant mass distribution can be used to measure the angular distributions of the background. They will need to be subtracted to obtain the polarization information of the signal from the events in the peak region.

To calculate the expected number of signal events, we computed the $pp \rightarrow c\bar{c}$ cross sections $\sigma_{c\bar{c}}$ with the jet trigger cuts from table 5 using a MadGraph simulation. In addition, for the c polarization measurements we require the c jet to contain a $\Lambda_c^+ \rightarrow pK^-\pi^+$ decay. For the spin correlations we require this Λ_c^+ decay in one jet and the analogous $\bar{\Lambda}_c^-$ decay in the other. The expected numbers of events for measurements of polarization (N_c) and spin correlations ($N_{c\bar{c}}$), calculated as

$$N_c = \mathcal{L} \sigma_{c\bar{c}} f(c \rightarrow \Lambda_c^+) \text{BR}(\Lambda_c^+ \rightarrow pK^-\pi^+) \epsilon_{\Lambda_c^+}, \quad (6.4)$$

$$N_{c\bar{c}} = \mathcal{L} \sigma_{c\bar{c}} f^2(c \rightarrow \Lambda_c^+) \text{BR}^2(\Lambda_c^+ \rightarrow pK^-\pi^+) \epsilon_{\Lambda_c^+}^2, \quad (6.5)$$

are shown in table 8 for Run 2 and the HL-LHC. We also provide results that correspond to different cuts on the dijet invariant mass, m_{jj} , as such cuts can enhance the sensitivity to new physics contributions. As can be seen in the table, the number of events available for the spin correlation measurements in this channel is small even for the HL-LHC (considering also the relatively low purity), so we proceed with the analysis of polarization measurements only. The table shows the expected statistical uncertainties for the polarization measurements (multiplied by the polarization retention factors) $r_i\Delta b_i^\pm$ based on eq. (4.18). The prospects are borderline for Run 2 but seem good for the HL-LHC.

6.3.2 Semileptonic Channel

A potentially more promising avenue is the semileptonic decay $\Lambda_c^+ \rightarrow \Lambda \mu^+ \nu_\mu$ with $\Lambda \rightarrow p\pi^-$. While the branching ratio of this decay chain (3.5% for $\Lambda_c^+ \rightarrow \Lambda \mu^+ \nu_\mu$, 64% for $\Lambda \rightarrow p\pi^-$ [42]) is lower than that of the hadronic decay, the muon triggers have very low p_T thresholds (see table 5) so there is a potential for getting more data. We do not consider a selection without a Λ decay reconstructed in the tracker because it will be difficult to extract the Λ_c^+ polarization information if the muon will be the only product associated with the Λ_c^+ decay. Besides that, the Λ requirement strongly suppresses the intrinsic background due to semileptonic D -meson decays since they are kinematically forbidden from producing a Λ (which would have to be produced together with an antibaryon, for baryon number conservation, while no sufficiently light antibaryons exist).

This channel also has disadvantages, such as the low reconstruction efficiency of Λ decays, and the shortness of the Λ_c^+ lifetime ($c\tau \approx 0.06$ mm) which leads to large uncertainties in its flight direction reconstruction, which is needed for the neutrino reconstruction. Although these challenges exist we will analyze the potential of this channel.

Our selection in this channel requires the jet to contain a muon (as done sometimes for charm jet tagging [50, 51, 106–108]) as well as a reconstructed $\Lambda \rightarrow p\pi^-$ decay. To ensure that the Λ originates from a Λ_c^+ decay, one should demand the Λ trajectory (inferred from the momenta of its decay products) to form a displaced vertex with the muon. Events in which the Λ trajectory is consistent with both a common vertex with the muon and the primary vertex, can still be accepted if the Λ carries a significant fraction (e.g., above 20%) of the jet momentum, since Λ baryons produced in parton showering and hadronization will usually be soft. We expect this requirement to have high signal efficiency and significant background suppression, but estimating the efficiency and purity quantitatively requires a detailed simulation which is beyond the scope of the current work.

There is an extrinsic background from $b\bar{b}$ production. We can estimate the size of this background by starting with the inclusive branching ratio for b jets to contain a Λ or $\bar{\Lambda}$ baryon, which was measured to be [42]

$$\text{BR}(b \rightarrow (b\text{-hadron}) \rightarrow \Lambda/\bar{\Lambda} + X) \approx (5.9 \pm 0.6)\%. \quad (6.6)$$

Accounting for us requiring a Λ (not a $\bar{\Lambda}$) while on the other hand collecting background from both the b and \bar{b} jet, we are left with the same number. We will further assume that the probability of having a μ^+ in association with the Λ is roughly 10%.⁹ The corresponding numbers are compared with the signal in table 9.

There are a number of ways to reduce the $b\bar{b}$ background significantly. One can immediately veto events in which both the secondary vertex from the b -hadron decay and the tertiary vertex from the subsequent charmed hadron decay can be distinguished. Moreover, one can use the order-of-magnitude difference between the Λ_c^+ and b -hadron lifetimes (see

⁹This assumption is based on the fact that the off-shell W boson that produces the muon can also produce other flavors of leptons and quarks, to the extent allowed by phase space. While the most common decay chain $b \rightarrow c \rightarrow s$ (for example) involves two W bosons, they produce muons of opposite charges, only one of which is relevant to our signal.

Fragmentation and Decay	FF [%]	BR [%]	FF×BR [%]	Lifetime [s]
Signal: $c \rightarrow \Lambda_c^+ \rightarrow \Lambda \mu^+ \nu_\mu$	6.4	3.5	0.22	$2.0 \cdot 10^{-13}$
Background:				
$b+\bar{b} \rightarrow (b \text{ and } \bar{b} \text{ hadrons}) \rightarrow \Lambda \mu^+ \nu_\mu X$			0.59	$1.6 \cdot 10^{-12}$
<i>based on:</i> $b \rightarrow (b\text{-hadron}) \rightarrow \Lambda/\bar{\Lambda} + X$			5.9	

Table 9: Properties of the semileptonic Λ_c^+ signal and the $b\bar{b}$ background: fragmentation fractions (FF) [44], branching ratios (BR) [42] and lifetimes [42]. The $c\bar{c}$ and $b\bar{b}$ production cross sections are similar for given cuts on the jets. The number shown for the background is already summed over the two jets in the event and involves the assumption that roughly 10% of the events in the ΛX sample contain a μ^+ . The numbers shown are before any discriminating cuts.

table 9) and apply an upper bound on the transverse displacement d_T of the secondary vertex. For example, requiring $d_T < 0.77 \text{ mm} \times (p_T^{\text{jet}}/115 \text{ GeV})$ has an efficiency of 40% for the signal and 10% for the background, giving 60% purity.¹⁰ Various additional discriminants between b and c jets exist and are used in c tagging algorithms. For a c -jet efficiency of 40%, a b -jet efficiency as low as 6% is achieved in both ATLAS [109] and CMS [50], which would lead to 71% purity in our case. The performance of charm tagging should be even better when applied to the Λ_c^+ sample than to an inclusive sample of charmed hadrons because the lifetimes of the more common charmed hadrons are closer to the b -hadron lifetimes. In addition, the properties of our decay of interest can suppress the background further. In particular, one can require that the displaced vertex formed by the muon track and the inferred Λ trajectory (if it is distinct from the primary vertex) should not contain any additional tracks. Based on these arguments, we will assume a charm tagging efficiency of $\epsilon_c \approx 40\%$ and neglect the remaining background.

Table 10 shows the Run 2 cross sections and numbers of events available for measurements of polarization (N_c) and spin correlations ($N_{c\bar{c}}$). The cross sections are based on the single muon trigger acceptance for the polarization and the double muon trigger for spin correlations. They were obtained using a Pythia simulation of $pp \rightarrow c\bar{c}$, where we allowed the charmed hadrons to decay only to final states with a muon and applied the trigger cuts from table 5 to muons from charmed hadrons inside the two leading jets. These cross sections do not include branching ratios. The numbers of events were calculated as

$$N_c = \mathcal{L} \sigma_{c\bar{c}} f(c \rightarrow \Lambda_c^+) \text{BR}(\Lambda_c^+ \rightarrow \Lambda \mu^+ \nu_\mu) \text{BR}(\Lambda \rightarrow p\pi^-) \epsilon_\mu \epsilon_c \epsilon_\Lambda, \quad (6.7)$$

$$N_{c\bar{c}} = \mathcal{L} \sigma_{c\bar{c}} f^2(c \rightarrow \Lambda_c^+) \text{BR}^2(\Lambda_c^+ \rightarrow \Lambda \mu^+ \nu_\mu) \text{BR}^2(\Lambda \rightarrow p\pi^-) \epsilon_{c,2} \epsilon_\Lambda^2, \quad (6.8)$$

where $\epsilon_\mu \approx 50\%$ is the efficiency for the muon to pass the isolation requirement of the single muon trigger [77], $\epsilon_{c,2} \equiv 2\epsilon_c - \epsilon_c^2$ is the efficiency for any of the two jets to pass charm tagging, and ϵ_Λ includes the decay radius and reconstruction efficiencies of the Λ , where

¹⁰To obtain these numbers we assumed that the jet p_T fraction carried by the hadron is 0.5 for the Λ_c^+ and 0.7 for the b hadrons.

$c\bar{c}$, semileptonic	polarization			spin correlations	
m_{jj} cut [GeV]	$\sigma_{c\bar{c}}$ [pb]	N_c	$r_i\Delta b_i^\pm$	$\sigma_{c\bar{c}}$ [pb]	$N_{c\bar{c}}$
no cut	2500	8.3×10^3	0.019	2300	3
100	2200	7.2×10^3	0.020	2000	2
300	350	1.2×10^3	0.051	250	
500	66	160	0.14	48	
750	14	22	0.37	9.3	

Table 10: Run 2 cross sections (with trigger-motivated cuts) and signal event counts (after the full selection) for measurements of c -quark polarization and spin correlations in the semileptonic channel. The expected statistical uncertainties for the polarization measurements are shown as well.

we again rely on the LRT algorithm [87–89]. As discussed in section 6.2.1, for Run 2, in the range of Λ decay radii d_T up to $d_T^{\max} \approx 300$ mm, the average reconstruction efficiency for each track is expected to be $\epsilon_{\text{track}} \approx 65\%$, and for the HL-LHC, in the range of up to $d_T^{\max} \approx 400$ mm, it will be $\epsilon_{\text{track}} \approx 80\%$. Averaging over the whole range is justified as the mean decay radius is $\langle d_T \rangle \gg d_T^{\max}$. We estimate $\langle d_T \rangle$ with the assumption that $p_T^\Lambda \sim (0.5/3)p_T^{\text{jet}}$, where the factor of 0.5 is the typical c -jet momentum fraction carried by the Λ_c^+ and the division by 3 roughly accounts for the Λ being one out of three decay products. For the jet p_T , we used the rough estimate $p_T^{\text{jet}} \sim \max(\bar{p}_T^{\text{jet}}, m_{jj}^{\text{cut}}/3)$ where $\bar{p}_T^{\text{jet}} \approx 115$ GeV is the cut on jets that is equivalent to the cuts of both the single and double muon triggers of Run 2, like we already discussed in a slightly different context in section 5. For the HL-LHC, the equivalent jet cuts are 85 GeV and 80 GeV for the single and double muon triggers, respectively.

Table 10 also shows the expected statistical uncertainty of the polarization measurements, while the number of events for spin correlation measurements in Run 2 is too small to be useful. Table 11 presents the analogous results for the HL-LHC, where spin correlation measurements become feasible. We see that the semileptonic channel is superior to the hadronic channel, except for polarization measurements at high m_{jj} at the HL-LHC, where the two channels are comparable.

6.3.3 Mixed Channel

We can also look at a mixed channel, where the decay in one of the jets is semileptonic and in the other hadronic. This channel combines the ability to trigger on a muon (with a low p_T threshold) on one side with the higher BR and a cleaner decay (without a neutrino) on the other side.

We propose using the hadronic side of the event for polarization measurements due to the ability to fully reconstruct the decay kinematics, without the need to account for a neutrino. Moreover, one can then enjoy the *inclusive* semimuonic decays of *all* charmed hadrons (see table 12) in the second jet to trigger the event. The expected number of signal

$c\bar{c}$, semilep.	polarization			spin correlations			
m_{jj} cut [GeV]	$\sigma_{c\bar{c}}$ [pb]	N_c	$r_i \Delta b_i^\pm$	$\sigma_{c\bar{c}}$ [pb]	$N_{c\bar{c}}$	$r_i^2 \Delta c_{ii}$	$r_i r_j \Delta c_{ij(\ell)}$
no cut	9400	1.7×10^6	0.001	13000	2.4×10^3	0.060	0.042
100	6700	1.2×10^6	0.002	7700	1.5×10^3	0.078	0.054
300	620	9.8×10^4	0.005	540	70	0.35	0.25
500	110	1.1×10^4	0.017	89	4		
750	23	1.6×10^3	0.043	16			
1000	5.4	280	0.10	4.1			
1500	0.62	22	0.37	0.47			

Table 11: HL-LHC cross sections (with trigger-motivated cuts) and signal event counts (after the full selection) for measurements of c -quark polarization and spin correlations in the semileptonic channel. The expected statistical uncertainties are shown as well. The shorthand $\Delta c_{ij(\ell)}$ denotes the uncertainties in c_{ij} and c_ℓ , which are of the same size.

h_c	$f(c \rightarrow h_c)$ [%]	BR($h_c \rightarrow \mu^+ X$) [%]
Λ_c^+	6.4	3.5
D^+	22.7	17.6
D^0	61.8	6.8
D_s^+	8.2	≈ 6

Table 12: The fragmentation fractions [44] and branching ratios [42] of inclusive semi-muonic decays of the common charmed hadrons.

events in the sample is then

$$\begin{aligned}
N_c = & \mathcal{L} \sigma_{c\bar{c}} f(c \rightarrow \Lambda_c^+) \text{BR}(\Lambda_c^+ \rightarrow pK^-\pi^+) \epsilon_{\Lambda_c^+ \rightarrow pK^-\pi^+} \\
& \times \sum_{h_c=\Lambda_c^+, D^+, D^0, D_s^+} f(c \rightarrow h_c) \text{BR}(h_c \rightarrow \mu^+ X) \epsilon_\mu,
\end{aligned} \tag{6.9}$$

where we assume an efficiency of $\epsilon_{\Lambda_c^+ \rightarrow pK^-\pi^+} \approx 25\%$ for the hadronic decay selection [100] and $\epsilon_\mu \approx 50\%$ for passing the isolation requirement of the single muon trigger [77]. The resulting numbers of events are given in table 13.

The requirement of the muon in the second jet is also expected to remove part of the background that is observed under the $\Lambda_c^+ \rightarrow pK^-\pi^+$ peak in the CMS measurement [100]. While it will not eliminate background coming from $c\bar{c}$ or $b\bar{b}$, the muon requirement will strongly suppress the combinatorial background from high cross section dijet final states without heavy flavors (e.g., gg). Since we do not know the composition of the background observed by CMS, we present in table 13 a range of values for the statistical uncertainties, for purities varying between 100% and the hadronic decay purity of 6.9% for Run 2 (as in

$c\bar{c}$, mixed channel, polarization						
m_{jj} cut [GeV]	Run 2			HL-LHC		
	$\sigma_{c\bar{c}}$ [pb]	N_c	$r_i\Delta b_i^\pm$	$\sigma_{c\bar{c}}$ [pb]	N_c	$r_i\Delta b_i^\pm$
no cut	2500	1.6×10^4	0.021 – 0.080	9400	1.3×10^6	0.002 – 0.006
100	2200	1.3×10^4	0.022 – 0.085	6700	9.0×10^5	0.003 – 0.007
300	350	2600	0.055 – 0.21	620	8.4×10^4	0.009 – 0.024
500	66	520	0.13 – 0.49	110	1.4×10^4	0.021 – 0.059
750	14	86	$\gtrsim 0.28$	23	3.1×10^3	0.047 – 0.13
1000	3.5	22		5.4	730	0.097 – 0.26
1500	0.40	2		0.62	84	$\gtrsim 0.29$

Table 13: Cross sections, expected numbers of signal events and expected statistical uncertainties for the c -quark polarization measurements using the hadronic decay in the mixed channel of $c\bar{c}$. We show a range of values for the statistical uncertainties, corresponding to purities between 100% and 6.9% for Run 2 and 13.8% for the HL-LHC (see text).

the CMS measurement) and 13.8% for the HL-LHC (recall the discussion in section 6.3.1). The results in table 13 are comparable to those of the semileptonic channel.

For spin correlation measurements, the expected number of signal events is

$$\begin{aligned}
N_{c\bar{c}} = & \mathcal{L} \sigma_{c\bar{c}} f^2(c \rightarrow \Lambda_c^+) \text{BR}(\Lambda_c^+ \rightarrow pK^-\pi^+) \text{BR}(\Lambda_c^+ \rightarrow \Lambda\mu^+\nu_\mu) \text{BR}(\Lambda \rightarrow p\pi^-) \\
& \times \epsilon_{\Lambda_c^+ \rightarrow pK^-\pi^+} \epsilon_\Lambda \epsilon_\mu \epsilon_c, \tag{6.10}
\end{aligned}$$

where $\epsilon_{\Lambda_c^+ \rightarrow pK^-\pi^+} \approx 25\%$ is the hadronic decay efficiency [100], ϵ_Λ describes the Λ decay acceptance and reconstruction efficiency (estimated as in section 6.3.2), $\epsilon_\mu \approx 50\%$ is the efficiency loss due to the isolation requirement of the single muon trigger [77], and ϵ_c is the charm tagging efficiency discussed in section 6.3.2. Table 14 shows the expected numbers of events for Run 2 and the HL-LHC. While the same single-muon trigger is used here as in the polarization measurements, the cross sections are higher by a factor of 2 because either a μ^+ from the c jet or a μ^- from the \bar{c} jet can trigger the event. This also affects the equivalent p_T^{jet} values we use to estimate the Λ displacement acceptance, which become $\bar{p}_T^{\text{jet}} = 97$ GeV for Run 2 and $\bar{p}_T^{\text{jet}} = 72$ GeV for the HL-LHC.

While the semileptonic decay selection is almost background-free (as discussed in section 6.3.2), various processes can mimic the hadronic decay. If the background observed under the hadronic Λ_c^+ peak in the inclusive CMS sample [100] is primarily intrinsic (i.e., from $c\bar{c}$), it will not be affected by the semileptonic selection on the other side of the event and our rough purity estimates will be 6.9% in Run 2 and 13.8% at the HL-LHC. If, on the other hand, the background is mostly extrinsic and comes from a process such as $pp \rightarrow gg$, where the jets rarely contain a muon and a Λ , the semileptonic selection will eliminate most of it and the sample will be almost background-free. For Run 2, the number of events is too small for a meaningful measurement regardless of the background. For the

$c\bar{c}$, mixed channel, spin correlations						
m_{jj} cut [GeV]	Run 2		HL-LHC			
	$\sigma_{c\bar{c}}$ [pb]	$N_{c\bar{c}}$	$\sigma_{c\bar{c}}$ [pb]	$N_{c\bar{c}}$	$r_i^2 \Delta c_{ii}$	$r_i r_j \Delta c_{ij(\ell)}$
no cut	5000	19	19000	3.9×10^3	0.072 – 0.19	0.050 – 0.13
100	4300	16	13000	2.7×10^3	0.085 – 0.23	0.060 – 0.16
300	710	2	1200	200	$\gtrsim 0.32$	$\gtrsim 0.22$

Table 14: Cross sections, expected numbers of signal events and expected statistical uncertainties for the $c\bar{c}$ spin correlation measurements in the mixed channel. We show a range of values for the statistical uncertainties, corresponding to purities between 100% and 13.8% (see text).

HL-LHC, we show in table 14 a range of values for the expected precision corresponding to the above range of possible purity values. The expected precision is comparable to that of the semileptonic channel.

6.4 Analyses of $pp \rightarrow b\bar{b}$

We propose using the $b \rightarrow \Lambda_b \rightarrow X_c \mu^- \bar{\nu}_\mu$ process, with the muon-based triggers from table 5, to measure the polarization and spin correlations in $b\bar{b}$ events.

As introduced in section 3, we will consider three types of selection: Inclusive, Semi-inclusive, and Exclusive. In the Inclusive Selection, no attempt is made to reduce the intrinsic background due to semileptonic B -meson decays. Such a selection can still be competitive because of its high signal efficiency. In the Semi-Inclusive selection, we require in addition to the muon the reconstruction of a Λ baryon (via its decay $\Lambda \rightarrow p\pi^-$) originating from the vicinity of the displaced vertex. This reduces the B -meson background. The last selection type is the Exclusive Selection. In this selection, in addition to the muon, we require a full reconstruction of one of Λ_c^+ decays by a set of tracks consistent with originating from a common vertex. This significantly suppresses the B -meson background too. Another advantage of the complete reconstruction of a Λ_c^+ decay is that the kinematics of the Λ_b decay as a whole can then be reconstructed more accurately. In table 15 we list all the decay channels relevant to the signal in each selection type.¹¹

6.4.1 Inclusive Selection

The main requirement of this selection is the presence a muon in the jet, similar to *soft muon b tagging* [49, 78, 106, 107, 115, 116].

To suppress extrinsic backgrounds with prompt or mildly displaced (in particular, $c\bar{c}$) muons, we assume applying a b tagging algorithm that may use the muon impact parameter significance, or p_T^{rel} (the component of muon momentum transverse to the jet axis) [106], or

¹¹In the Exclusive Selection, we include decays with the Σ^\pm baryons in the final state. While these particles will often decay before passing through the entire tracker, reconstruction of such short tracks is possible [110–114].

Selection	Decay Modes	Branching Ratio
Inclusive	$\Lambda_b \rightarrow X_c \mu^- \bar{\nu}_\mu$	11%
Semi-inclusive	$\Lambda_c^+ \rightarrow \Lambda X$	38%
	$\Lambda \rightarrow p \pi^-$	64%
Exclusive	$\Lambda_c^+ \rightarrow p K^- \pi^+$	6.3%
	$\Lambda_c^+ \rightarrow \Lambda \pi^+ \rightarrow p \pi^- \pi^+$	0.8%
	$\Lambda_c^+ \rightarrow p K_S \rightarrow p \pi^- \pi^+$	1.1%
	$\Lambda_c^+ \rightarrow \Lambda \pi^+ \pi^+ \pi^- \rightarrow p \pi^+ \pi^+ \pi^- \pi^-$	2.3%
	$\Lambda_c^+ \rightarrow p K_S \pi^+ \pi^- \rightarrow p \pi^+ \pi^+ \pi^- \pi^-$	1.1%
	$\Lambda_c^+ \rightarrow \Sigma^+ \pi^+ \pi^-$	4.5%
	$\Lambda_c^+ \rightarrow \Sigma^- \pi^+ \pi^+$	1.9%
	total	18%

Table 15: Decay modes relevant to the three Λ_b selections and their branching ratios [42]. The Semi-inclusive and Exclusive selections are done on top of the Inclusive selection.

other variables. For our estimates, we will assume the b tagging efficiency to be $\epsilon_b \approx 80\%$ and allow ourselves to neglect the above backgrounds.

Another source of extrinsic background is $pp \rightarrow t\bar{t} \rightarrow b\bar{b}X$. This background will be small since the $t\bar{t}$ cross section is smaller than the $b\bar{b}$ cross section for any fixed $b\bar{b}$ invariant mass. It can be suppressed further by vetoing the presence of additional objects such as isolated leptons or multiple energetic jets.

The intrinsic background is the more prominent one. An important contribution is made by the semileptonic B -meson decays via the same underlying process as in the signal, $b \rightarrow c \mu^- \bar{\nu}_\mu$, but we do not attempt to reduce it in the inclusive selection as we want to keep the signal efficiency high. Another source of intrinsic background is the decay chain $b \rightarrow c f \bar{f}'$, $c \rightarrow s \mu^+ \nu_\mu$. The fact that the muon in this case has the wrong charge cannot be used to eliminate this background because in the inclusive selection we do not know which jet is coming from the b and which from the \bar{b} . There is a different way to reduce this background significantly. The muons emitted in $b \rightarrow c$ transitions (as in our signal) are usually more energetic than those emitted in the $c \rightarrow s$ transitions in the $b \rightarrow c \rightarrow s$ chain (which are background), so it can be useful to look into the ratio between the muon and jet p_T , $z = p_T^\mu / p_T^{\text{jet}}$. Figure 4 shows the z distributions for muons from both b and c hadrons in $pp \rightarrow b\bar{b}$ events with $\sqrt{s} = 13$ TeV simulated in Pythia with the single-muon trigger cuts. In a sample without any further cuts, the contribution of muons from c -hadron decays is small to begin with, due to their lower efficiency to pass the trigger p_T cut. For a dijet invariant mass cut of $m_{jj} > 1000$ GeV, their relative contribution is significant, but concentrated at lower values of z than the muons from b hadrons. Based on these results, we will apply a cut of $z > 0.2$ in all cases. In the example with the $m_{jj} > 1000$ GeV cut,

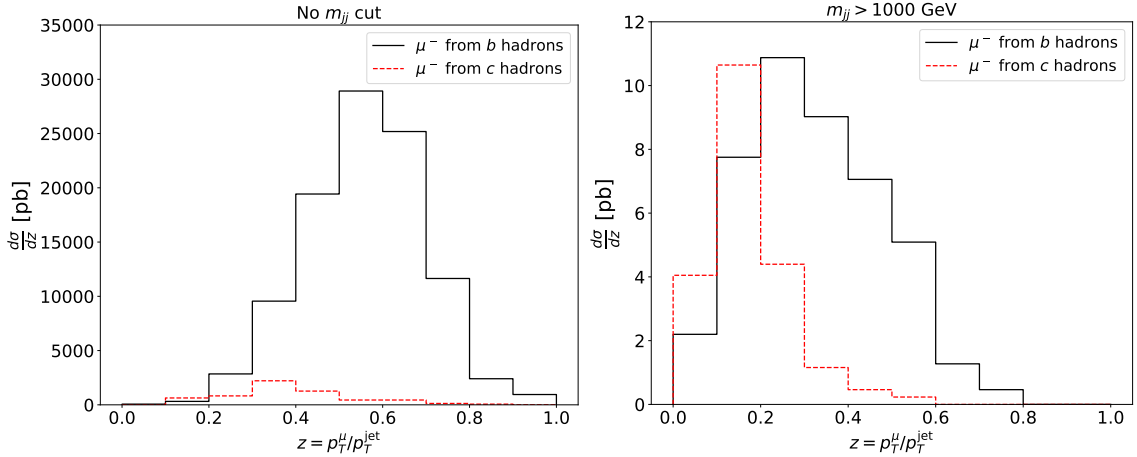


Figure 4: The momentum fraction z of the muons relative to their respective jets. The graphs compare the distributions for muons originating directly from b hadrons with those from c hadrons in b jets, with no invariant mass cut (left) and with $m_{jj} > 1000$ GeV (right). (The plot normalizations do not include the branching ratios.)

this z cut results in decent efficiency and purity ($\epsilon_z \approx 77\%$, $f_z \approx 84\%$), while the impact on the no-cut case is small ($\epsilon_z \approx 99\%$, $f_z \approx 94\%$). From these results, we find that the c hadrons background is small and we will neglect it.

The numbers of events available for measurements of polarization and spin correlations, respectively, are given by

$$N_b^i = \mathcal{L} \sigma_{b\bar{b}} f(b \rightarrow \Lambda_b) \text{BR}(\Lambda_b \rightarrow X_c \mu^- \bar{\nu}_\mu) \epsilon_b \epsilon_z \epsilon_\mu, \quad (6.11)$$

$$N_{b\bar{b}}^{ii} = \mathcal{L} \sigma_{b\bar{b}} f^2(b \rightarrow \Lambda_b) \text{BR}^2(\Lambda_b \rightarrow X_c \mu^- \bar{\nu}_\mu) \epsilon_{b,2} \epsilon_{z,2}, \quad (6.12)$$

where $\epsilon_\mu \approx 50\%$ is the efficiency for the muon to pass the isolation requirement of the single muon trigger [77], $\epsilon_{b,2} \equiv 2\epsilon_b - \epsilon_b^2$ is the efficiency for any of the two jets to pass the b tagging condition, and $\epsilon_{z,2} \equiv 2\epsilon_z - \epsilon_z^2$ is the efficiency for any of the two muons to pass the momentum fraction cut.¹² The cross sections were obtained using a Pythia simulation of $pp \rightarrow b\bar{b}$, where we allowed the bottom hadrons to decay only to final states with a muon (not including cases in which the muon comes from a charmed hadron) and applied the single or double muon trigger cuts from table 5 to muons from bottom hadrons inside the two leading jets. These cross sections do not include branching ratios. The resulting numbers of events are shown in tables 16 and 17 for Run 2 and the HL-LHC, respectively, along with the numbers obtained for the other selections. While here we considered the standard muon-based triggers, table 16 also presents numbers corresponding to the CMS parked dataset. It will be discussed separately in section 6.4.5.

By accounting for the fragmentation fractions and semi-muonic decay branching ratios of the \bar{B}^0 , B^- , and \bar{B}_s^0 mesons (see table 18), we estimate the sample purity to be $f \approx 7.4\%$

¹²Once one of the muons is classified as signal, the second muon can be classified as signal or background based on its charge.

m_{jj} cut [GeV]	$\sigma_{b\bar{b}}$ [pb]	N_b^i	N_b^s	N_b^e
no cut	9400	4.0×10^6	2.0×10^5	3.6×10^5
100	7200	3.1×10^6	1.5×10^5	2.8×10^5
300	560	2.3×10^5	1.0×10^4	2.1×10^4
500	82	3.1×10^4	1.0×10^3	2.8×10^3
750	14	4.8×10^3	120	430
1000	3.4	1.1×10^3	22	100
1500	0.34	100		9
parked data		3.5×10^8	3.6×10^7	3.1×10^7
purity f [%]		7.4	57	66

(a) Polarization

m_{jj} cut [GeV]	$\sigma_{b\bar{b}}$ [pb]	$N_{b\bar{b}}^{ii}$	$N_{b\bar{b}}^{ss}$	$N_{b\bar{b}}^{ee}$	$N_{b\bar{b}}^{is}$	$N_{b\bar{b}}^{ie}$	$N_{b\bar{b}}^{se}$
no cut	10000	8.0×10^4	200	640	8.1×10^3	1.4×10^4	730
100	5900	4.7×10^4	121	380	4.8×10^3	8.5×10^3	430
300	340	2.7×10^3	4	21	230	490	20
500	46	360		2	20	65	1
parked data		1.1×10^6	1.1×10^4	8700	2.2×10^5	1.9×10^5	2.0×10^4
purity f [%]		0.55	32	44	4.2	4.9	38

(b) Spin correlations

Table 16: Run 2 cross sections (with trigger-motivated cuts) and signal event counts (after the full selection) for measurements of (a) b -quark polarization, and (b) $b\bar{b}$ spin correlations in the inclusive, semi-inclusive, and exclusive selection channels. The last row shows the expected sample purity.

for a single jet. For spin correlation measurements, which involve two jets, this number is squared, giving the purity of $f \approx 0.55\%$. Such a low purity can be problematic as it means that even a small mismodelling of the background can ruin the measurement. The next two selection strategies that we discuss offer much higher purities, at the expense of statistics.

6.4.2 Exclusive Selection

The exclusive selection starts with the inclusive selection and requires, in addition, a fully reconstructed Λ_c^+ decay, to eliminate most of the background due to the semileptonic B -meson decays, which usually produce charmed mesons rather than baryons.

m_{jj} cut [GeV]	$\sigma_{b\bar{b}}$ [pb]	N_b^i	N_b^s	N_b^e
no cut	33000	3.0×10^8	3.3×10^7	2.7×10^7
100	18300	1.7×10^8	1.8×10^7	1.5×10^7
300	990	8.2×10^6	7.3×10^5	7.4×10^5
500	126	9.3×10^5	6.3×10^4	8.4×10^4
750	21	1.5×10^5	7.6×10^3	1.4×10^4
1000	5.6	3.7×10^4	1.6×10^3	3.3×10^3
1500	0.49	2.9×10^3	94	260
2000	0.088	490	12	44
purity f [%]		7.4	57	66

(a) Polarization

m_{jj} cut [GeV]	$\sigma_{b\bar{b}}$ [pb]	$N_{b\bar{b}}^{ii}$	$N_{b\bar{b}}^{ss}$	$N_{b\bar{b}}^{ee}$	$N_{b\bar{b}}^{is}$	$N_{b\bar{b}}^{ie}$	$N_{b\bar{b}}^{se}$
no cut	39000	6.7×10^6	8.1×10^4	5.4×10^4	1.5×10^6	1.2×10^6	1.3×10^5
100	15000	2.6×10^6	3.1×10^4	2.1×10^4	5.7×10^5	4.7×10^5	5.1×10^4
300	570	9.6×10^4	610	780	1.5×10^4	1.7×10^4	1.4×10^3
500	74	1.2×10^4	35	98	1.3×10^3	2.2×10^3	120
750	12	2.0×10^3	3	16	150	360	13
1000	2.9	460		3	27	82	2
purity f [%]		0.55	32	44	4.2	4.9	38

(b) Spin correlations

Table 17: HL-LHC cross sections (with trigger-motivated cuts) and signal event counts (after the full selection) for measurements of (a) b -quark polarization, and (b) $b\bar{b}$ spin correlations in the inclusive, semi-inclusive, and exclusive selection channels. The last row shows the expected sample purity.

Process	FF [%]	BR [%]
$b \rightarrow \Lambda_b \rightarrow \mu^- \bar{\nu}_\mu X$	7.0	11
$b \rightarrow \bar{B}^0 \rightarrow \mu^- \bar{\nu}_\mu X$	40.1	10.3
$b \rightarrow B^- \rightarrow \mu^- \bar{\nu}_\mu X$	40.1	11.0
$b \rightarrow \bar{B}_s^0 \rightarrow \mu^- \bar{\nu}_\mu X$	10.4	10.2

Table 18: The fragmentation fractions (FF) [18, 117] and branching ratios (BR) [42] of the signal (Λ_b) and the intrinsic background in the Inclusive Selection.

Process	FF [%]	BR [%]
$b \rightarrow \Lambda_b \rightarrow \Lambda_c^+ X$	7.0	≈ 100
$b \rightarrow B^- \rightarrow \Lambda_c^+ X$	40.1	$2.8_{-0.9}^{+1.1}$
$b \rightarrow \bar{B}^0 \rightarrow \Lambda_c^+ X$	40.1	$5.0_{-1.5}^{+2.1}$
$b \rightarrow \bar{B}_s^0 \rightarrow \Lambda_c^+ X$	10.4	unknown
$\bar{b} \rightarrow B^+ \rightarrow \Lambda_c^+ X$	40.1	$2.1_{-0.6}^{+0.9}$
$\bar{b} \rightarrow B^0 \rightarrow \Lambda_c^+ X$	40.1	< 3.1
$\bar{b} \rightarrow B_s^0 \rightarrow \Lambda_c^+ X$	10.4	unknown

Table 19: The fragmentation fractions (FF) [18, 117] and branching ratios (BR) [42] for Λ_c^+ production from the Λ_b (signal) and B mesons (background).

Some of the Λ_c^+ decay channels listed in table 15 come with an efficiency price: K_S and Λ can decay too far to be reconstructed, Σ^\pm can produce a kinked track, and the channels with five tracks need each track to be successfully reconstructed. To account for this, as a rough estimate, we will assume a reconstruction efficiency of $\epsilon_{\text{reco}} \approx 50\%$ for the Λ_c^+ decays.

The numbers of events available for measurements of polarization and spin correlations, respectively, using the exclusive channel are given by

$$N_b^e = \mathcal{L} \sigma_{b\bar{b}} f(b \rightarrow \Lambda_b) \text{BR}(\Lambda_b \rightarrow X_c \mu^- \bar{\nu}_\mu) \text{BR}(\Lambda_c^+ \rightarrow \text{reco.}) \epsilon_b \epsilon_z \epsilon_{\text{reco}} \epsilon_\mu, \quad (6.13)$$

$$N_{b\bar{b}}^{ee} = \mathcal{L} \sigma_{b\bar{b}} f^2(b \rightarrow \Lambda_b) \text{BR}^2(\Lambda_b \rightarrow X_c \mu^- \bar{\nu}_\mu) \text{BR}^2(\Lambda_c^+ \rightarrow \text{reco.}) \epsilon_{b,2} \epsilon_{z,2} \epsilon_{\text{reco}}^2, \quad (6.14)$$

where $\text{BR}(\Lambda_c^+ \rightarrow \text{reco.}) \approx 18\%$ is the branching fraction of the reconstructible decay modes of the Λ_c^+ from table 15 and $\epsilon_\mu \approx 50\%$ is the efficiency for the muon to pass the isolation requirement of the single muon trigger [77]. The resulting numbers of events are included in tables 16 and 17.

A remaining background in this channel is the semileptonic decays of B mesons to final states with a Λ_c^+ baryon. While the branching ratios of the meson decays to baryons are small, their contribution is enhanced by their large fragmentation fractions compared with that of the Λ_b , as shown in table 19. The branching ratios for B -meson decays involving a μ^- in addition to the Λ_c^+ have not been measured, but such decays definitely exist. In the case of the b initial state, the muon can be produced in the $b \rightarrow (c \rightarrow \Lambda_c^+)$ transition, while in the case of the \bar{b} initial state is it produced following the $\bar{b} \rightarrow \bar{c} (c \rightarrow \Lambda_c^+) \bar{s}$ chain, in the subsequent $\bar{c} \rightarrow \bar{s}$ transition. Events with muons from the latter source will largely fail the cut on the muon momentum fraction z discussed in section 6.4.1, so only the B^- , \bar{B}^0 and \bar{B}_s^0 decays from table 19 actually contribute to the background. Summing up their contributions (while assigning \bar{B}_s^0 the average of the B^- and \bar{B}^0 BRs) and assuming the probability of having a muon to be similar to the Λ_b case, where the muon is also produced in a $b \rightarrow c$ transition, we obtain a sample purity of $f = 66\%$. Since the muons and neutrinos in these background processes are produced in the decays of spinless mesons, their impact on the angular distributions will be trivial.

6.4.3 Semi-inclusive Selection

The semi-inclusive selection starts with the inclusive selection and requires, in addition, the presence of a reconstructed Λ baryon. This requirement eliminates most of the contributions from B -meson decays while accepting a large fraction of Λ_b decays since Λ_b decays usually proceed through a Λ_c^+ , which in turn produces a Λ in about 38% of the cases [42].

The numbers of events in this channel, for measurements of polarization and spin correlations, respectively, are given by

$$N_b^s = \mathcal{L} \sigma_{b\bar{b}} f(b \rightarrow \Lambda_b) \text{BR}(\Lambda_b \rightarrow X_c \mu^- \bar{\nu}_\mu) \text{BR}(\Lambda_c^+ \rightarrow \Lambda X) \text{BR}(\Lambda \rightarrow p \pi^-) \epsilon_b \epsilon_z \epsilon_\Lambda \epsilon_\mu, \quad (6.15)$$

$$N_{b\bar{b}}^{ss} = \mathcal{L} \sigma_{b\bar{b}} f^2(b \rightarrow \Lambda_b) \text{BR}^2(\Lambda_b \rightarrow X_c \mu^- \bar{\nu}_\mu) \text{BR}^2(\Lambda_c^+ \rightarrow \Lambda X) \text{BR}^2(\Lambda \rightarrow p \pi^-) \epsilon_{b,2} \epsilon_{z,2} \epsilon_\Lambda^2, \quad (6.16)$$

where $\epsilon_\mu \approx 50\%$ is the efficiency for the muon to pass the isolation requirement of the single muon trigger [77] and ϵ_Λ is the Λ decay reconstruction efficiency, where we base our estimates on the ATLAS reconstruction with the LRT algorithm discussed in section 6.2.1. The mean track reconstruction efficiency is $\sim 65\%$ ($\sim 80\%$) in the range of decay radii up to 300 mm (400 mm) for Run 2 (HL-LHC). The typical b -jet p_T corresponding to the muons in the jets passing the double-muon trigger is $\bar{p}_T^{\text{jet}} \approx 79$ GeV (59 GeV) for Run 2 (HL-LHC). For the single-muon trigger it is 81 GeV (62 GeV) for Run 2 (HL-LHC). By an analytical calculation we find that with¹³ $p_T^\Lambda \sim (0.7/3^2) p_T^{\text{jet}}$, 54% of the Λ satisfy the decay radius condition for the Run 2 (with $p_T^{\text{jet}} = 79$ GeV) and 76% satisfy it for the HL-LHC (with $p_T^{\text{jet}} = 59$ GeV). This efficiency will be lowered significantly when we apply high invariant mass cuts. We account for that by taking $p_T^{\text{jet}} \sim \max(\bar{p}_T^{\text{jet}}, m_{jj}^{\text{cut}}/3)$ in our estimate of the typical p_T^Λ . The resulting numbers of events are included in tables 16 and 17.

The background in this channel can be estimated using the inclusive measurement of Λ baryon production in b -hadron decays, after subtracting the signal contribution. We have already discussed this measurement, eq. (6.6), in section 6.3.2 in the context of the background for the semileptonic $c\bar{c}$ channel. Following similar arguments, including an assumption of a 10% probability of having a μ^- alongside the Λ (as a rough estimate), we obtain the number “*Total*” in the second row in table 20. Part of it is the signal contribution, which is shown in the first row of the table. After subtracting it, we are left with the background, which is shown in the third row. The last row shows an estimate for the part of the background coming from processes involving the Λ_c^+ that are listed in table 19.¹⁴ This contribution seems to account for the majority of the background (although one should keep in mind the large uncertainties in the input data and the assumptions made). As we discussed in section 6.4.2, only the b -initiated processes from table 19, which account for roughly 60% of the background contributions in that table, will pass the cut

¹³The factor of 0.7 is the typical b -jet momentum fraction carried by a b hadron, and the $1/3^2$ factor is a rough estimate of the momentum splitting in a typical semileptonic Λ_b decay and the subsequent Λ_c^+ decay.

¹⁴For the B^0 BR, we took its upper bound. For the B_s^0 and \bar{B}_s^0 , we took the BR to be the average of the other BRs.

	Process	FF [%]	BR [%]	FF×BR [%]
<i>Signal</i>	$b \rightarrow \Lambda_b \rightarrow \Lambda \mu^- \bar{\nu}_\mu X$	7.0	3.8	0.29
<i>Total</i>	$b+\bar{b} \rightarrow (\text{hadrons}) \rightarrow \Lambda \mu^- \bar{\nu}_\mu X$			0.59
<i>Background</i>				0.30
via Λ_c^+	$b+\bar{b} \rightarrow (\text{mesons}) \rightarrow (\Lambda_c^+ \rightarrow \Lambda X) \mu^- \bar{\nu}_\mu X$			0.20

Table 20: Properties of the $b\bar{b}$ signal and background in the semi-inclusive channel: fragmentation fractions (FF) and branching ratios (BR). The number shown for *Total* is already summed over the two jets in the event and involves the assumption that roughly 10% of the events in the ΛX sample contain a μ^- . The *Background* number is obtained as the difference between *Total* and *Signal*. The last row shows the part of the background that comes from the processes involving the Λ_c^+ shown in table 19.

on the muon p_T fraction z . After subtracting that contribution we obtain a sample purity of $f \approx 57\%$.

6.4.4 Mixed Selections

For spin correlation measurements, one can also consider one type of selection (inclusive, semi-inclusive, or exclusive) for one of the jets and another type for another. The numbers of events for these mixed selections are given by

$$N_{bb}^{is} = 2 \mathcal{L} \sigma_{b\bar{b}} f^2(b \rightarrow \Lambda_b) \text{BR}^2(\Lambda_b \rightarrow X_c \mu^- \bar{\nu}_\mu) \text{BR}(\Lambda_c^+ \rightarrow \Lambda X) \text{BR}(\Lambda \rightarrow p\pi^-) \epsilon_{b,2} \epsilon_{z,2} \epsilon_\Lambda, \quad (6.17)$$

$$N_{bb}^{ie} = 2 \mathcal{L} \sigma_{b\bar{b}} f^2(b \rightarrow \Lambda_b) \text{BR}^2(\Lambda_b \rightarrow X_c \mu^- \bar{\nu}_\mu) \text{BR}(\Lambda_c^+ \rightarrow \text{reco.}) \epsilon_{b,2} \epsilon_{z,2} \epsilon_{\text{reco}}, \quad (6.18)$$

$$N_{bb}^{se} = 2 \mathcal{L} \sigma_{b\bar{b}} f^2(b \rightarrow \Lambda_b) \text{BR}^2(\Lambda_b \rightarrow X_c \mu^- \bar{\nu}_\mu) \text{BR}(\Lambda_c^+ \rightarrow \Lambda X) \text{BR}(\Lambda \rightarrow p\pi^-) \\ \times \text{BR}(\Lambda_c^+ \rightarrow \text{reco.}) \epsilon_{b,2} \epsilon_{z,2} \epsilon_\Lambda \epsilon_{\text{reco}} \quad (6.19)$$

for the inclusive/semi-inclusive, inclusive/exclusive and semi-inclusive/exclusive selections, respectively. We included a factor of two since different selections can be applied to each of the jets interchangeably and contribute the same. The resulting numbers are included in tables 16 and 17.

6.4.5 CMS Parked Data

It is also interesting to consider the CMS *parked* b dataset, which was collected during part of Run 2 using a special data acquisition strategy [36, 37].¹⁵ The dataset contains about $N_0 = 10^{10}$ $pp \rightarrow b\bar{b}$ events, in which one side of the event includes a displaced muon that triggered the event, with a p_T threshold that varied between 7 and 12 GeV. We will consider using these semileptonic decays with muons for the b and \bar{b} polarization measurements. We

¹⁵Similar data parking was done during part of Run 3 [118]. We are unaware of the specifics of data parking that might be planned for the HL-LHC, so we will not address that case. We hope that the analyses we propose in this paper, for the b , c , and s quarks, will add to the motivation for such data streams.

will also consider spin correlation measurements, in which we will demand a semileptonic decay with a muon also on the other side of the event.

The number of events available for the polarization measurements with the inclusive selection is

$$N_b^i \simeq \frac{1}{2} f(b \rightarrow \Lambda_b) N_0 \approx 3.5 \times 10^8, \quad (6.20)$$

where we accounted for the fact that only half of the triggering decays come from a b (while the other half are from a \bar{b}) and took the approximation that the inclusive semileptonic branching ratios and muon kinematics are approximately the same for the different b hadrons. We neglect the contribution of muons from the $b \rightarrow c \rightarrow \mu$ chain relative to the contribution of the direct $b \rightarrow \mu$ process since the more energetic muons from the direct decay pass the trigger threshold much more easily, similar to what we have seen in figure 4 (left). For the semi-inclusive and exclusive selections, we compute the number of events as follows:

$$N_b^s = N_b^i \text{BR}(\Lambda_c^+ \rightarrow \Lambda X) \text{BR}(\Lambda \rightarrow p\pi^-) \epsilon_\Lambda, \quad (6.21)$$

$$N_b^e = N_b^i \text{BR}(\Lambda_c^+ \rightarrow \text{reco.}) \epsilon_{\text{reco.}}. \quad (6.22)$$

For the semi-inclusive selection, our rough estimate for the Λ reconstruction efficiency, ϵ_Λ , will be as follows. Since the muon that triggers the event, with a p_T threshold that varied between 7 and 12 GeV [36, 37], is produced in the Λ_b decay together with the Λ_c^+ , which subsequently decays to the Λ and additional particles, we estimate p_T^Λ to be around a few GeV. As a result, the Λ baryons will usually decay sufficiently early to be reconstructed by an analogue of the LRT algorithm [87–89], but not at the shortest distances where the efficiency is maximal. We will therefore take $\epsilon_\Lambda \simeq \epsilon_{\text{track}}^2$ with $\epsilon_{\text{track}} \approx 65\%$ as a ballpark figure.

Our rough estimate for the number of events for the spin correlation measurement with the inclusive selection on both sides will be

$$N_{bb}^{ii} \simeq f^2(b \rightarrow \Lambda_b) \text{BR}(\Lambda_b \rightarrow X_c \mu^- \bar{\nu}_\mu) \mathcal{A} \epsilon N_0 \approx 1.1 \times 10^6, \quad (6.23)$$

where we took a ballpark figure of $\mathcal{A} \epsilon \sim 0.2$ for the acceptance times efficiency on the non-triggering side of the event (including the acceptance in η). The contribution of $b \rightarrow c \rightarrow \mu$ decays from that side of the event can be eliminated based on the muon charge (compared with the triggering muon). For the other selections, we have

$$N_{bb}^{ss} = N_{bb}^{ii} \text{BR}^2(\Lambda_c^+ \rightarrow \Lambda X) \text{BR}^2(\Lambda \rightarrow p\pi^-) \epsilon_\Lambda^2, \quad (6.24)$$

$$N_{bb}^{ee} = N_{bb}^{ii} \text{BR}^2(\Lambda_c^+ \rightarrow \text{reco.}) \epsilon_{\text{reco.}}^2, \quad (6.25)$$

$$N_{bb}^{is} = 2N_{bb}^{ii} \text{BR}(\Lambda_c^+ \rightarrow \Lambda X) \text{BR}(\Lambda \rightarrow p\pi^-) \epsilon_\Lambda, \quad (6.26)$$

$$N_{bb}^{ie} = 2N_{bb}^{ii} \text{BR}(\Lambda_c^+ \rightarrow \text{reco.}) \epsilon_{\text{reco.}}, \quad (6.27)$$

$$N_{bb}^{se} = 2N_{bb}^{ii} \text{BR}(\Lambda_c^+ \rightarrow \Lambda X) \text{BR}(\Lambda \rightarrow p\pi^-) \text{BR}(\Lambda_c^+ \rightarrow \text{reco.}) \epsilon_\Lambda \epsilon_{\text{reco.}}. \quad (6.28)$$

6.4.6 Expected Precision

The expected precision of the $b\bar{b}$ polarization and spin correlation measurements for either a muon or neutrino spin analyzer can be computed using eqs. (4.18)–(4.20). As indicated in

table 1, the neutrino in the Λ_b decay has a larger spin analyzing power than the muon and therefore has the potential to provide higher precision. Since the neutrino is not observed directly, a reconstruction is required, and it requires certain approximations, as discussed at the end of section 3. However, the decay reconstruction is needed anyway, even if the muon is used as the spin analyzer. We will therefore present the statistical uncertainties that can be obtained with the neutrino. The analogous results for the muon can be obtained by dividing the polarization uncertainties by $|\alpha_{\mu^-}|$ and the spin correlation uncertainties by $\alpha_{\mu^-}^2$, where $\alpha_{\mu^-} \approx -0.26$.

Table 21 shows the expected uncertainties for Run 2, for both the standard datasets and the CMS parked data. The results are promising for the polarization, and with the parked data also for the spin correlations. Analogous results for the HL-LHC are presented in table 22.

7 Summary and Discussion

In this work, we analyzed the feasibility of measuring quark polarization and spin correlations in high-energy $pp \rightarrow q\bar{q}$ events in ATLAS or CMS, where the quark q is b , c , or s . Such measurements can be done using the decay angular distributions of baryons produced from these quarks. Our main results are as follows:

- ◆ In the b -quark case, Run 2 data allows measuring the polarization in a number of channels of semileptonic Λ_b decays, with dijet invariant mass cuts up to ~ 1 TeV. Particularly precise measurements are possible with the CMS parked data. Spin correlation measurements are also feasible in multiple channels, although the statistical uncertainties will be sizable with the standard Run 2 datasets. An opportunity to do more precise measurements is again offered by the Run 2 CMS parked dataset.
- ◆ For the c quark, polarization measurements with Λ_c^+ decays using either the semileptonic or mixed channel are possible with the Run 2 dataset, and they can be extended to dijet invariant masses above 1 TeV at the HL-LHC using the same channels or the hadronic channel. Spin correlation measurements will be feasible at the HL-LHC in the semileptonic and mixed channels.
- ◆ The s -quark case is challenging in terms of the statistics that can be collected with the standard triggers. Polarization measurements become only borderline feasible with the statistics of the HL-LHC, and systematic uncertainties may pose challenges as well due to the low purity of the sample. There will not be enough statistics for $s\bar{s}$ spin correlation measurements even at the HL-LHC.

In table 23, we provide a more detailed summary of the measurement channels we have considered, showing in which of them a measurement is expected to be possible.

We would like to note that doing this broad survey of the different possible analysis channels required us to use various assumptions and approximations, as we described along the way. Therefore, our predicted sensitivities should be viewed as rough estimates. The

channel \rightarrow	inclusive	inclusive/inclusive		inclusive/exclusive	
m_{jj} cut [GeV]	$r_i \Delta b_i^\pm$	$r_i^2 \Delta c_{ii}$	$r_i r_j \Delta c_{ij(\ell)}$	$r_i^2 \Delta c_{ii}$	$r_i r_j \Delta c_{ij(\ell)}$
no cut	0.003	0.14	0.10	0.11	0.079
100	0.004	0.18	0.13	0.15	0.10
300	0.013				
500	0.036				
750	0.093				
1000	0.19				
parked data	0.0003	0.039	0.027	0.031	0.022

channel \rightarrow	semi-inclusive	semi-inclusive/semi-inclusive		semi-inclusive/inclusive	
m_{jj} cut [GeV]	$r_i \Delta b_i^\pm$	$r_i^2 \Delta c_{ii}$	$r_i r_j \Delta c_{ij(\ell)}$	$r_i^2 \Delta c_{ii}$	$r_i r_j \Delta c_{ij(\ell)}$
no cut	0.005	0.36	0.25	0.16	0.11
100	0.006	0.47	0.33	0.21	0.15
300	0.022				
500	0.072				
750	0.21				
parked data	0.0004	0.050	0.035	0.031	0.022

channel \rightarrow	exclusive	exclusive/exclusive		exclusive/semi-inclusive	
m_{jj} cut [GeV]	$r_i \Delta b_i^\pm$	$r_i^2 \Delta c_{ii}$	$r_i r_j \Delta c_{ij(\ell)}$	$r_i^2 \Delta c_{ii}$	$r_i r_j \Delta c_{ij(\ell)}$
no cut	0.003	0.18	0.11	0.18	0.13
100	0.004	0.23	0.16	0.23	0.16
300	0.015				
500	0.040				
750	0.10				
1000	0.21				
parked data	0.0004	0.049	0.034	0.034	0.024

Table 21: Expected statistical uncertainties for the polarization and spin correlation measurements in $b\bar{b}$ in Run 2 with a neutrino spin analyzer for different selection channels. The shorthand $\Delta c_{ij(\ell)}$ denotes the uncertainties in c_{ij} and c_ℓ , which are of the same size.

channel \rightarrow	inclusive	inclusive/inclusive		inclusive/exclusive	
m_{jj} cut [GeV]	$r_i \Delta b_i^\pm$	$r_i^2 \Delta c_{ii}$	$r_i r_j \Delta c_{ij(\ell)}$	$r_i^2 \Delta c_{ii}$	$r_i r_j \Delta c_{ij(\ell)}$
no cut	0.0004	0.015	0.011	0.012	0.0086
100	0.0005	0.025	0.017	0.020	0.014
300	0.0022	0.13	0.091	0.10	0.071
500	0.0063	0.36	0.26	0.29	0.20
750	0.016				
1000	0.032				
1500	0.11				
2000	0.27				

channel \rightarrow	semi-inclusive	semi-inclusive/semi-inclusive		semi-inclusive/inclusive	
m_{jj} cut [GeV]	$r_i \Delta b_i^\pm$	$r_i^2 \Delta c_{ii}$	$r_i r_j \Delta c_{ij(\ell)}$	$r_i^2 \Delta c_{ii}$	$r_i r_j \Delta c_{ij(\ell)}$
no cut	0.0004	0.018	0.013	0.012	0.0084
100	0.0005	0.029	0.021	0.019	0.013
300	0.0027	0.21	0.15	0.12	0.082
500	0.0091				
750	0.026				
1000	0.058				
1500	0.24				

channel \rightarrow	exclusive	exclusive/exclusive		exclusive/semi-inclusive	
m_{jj} cut [GeV]	$r_i \Delta b_i^\pm$	$r_i^2 \Delta c_{ii}$	$r_i r_j \Delta c_{ij(\ell)}$	$r_i^2 \Delta c_{ii}$	$r_i r_j \Delta c_{ij(\ell)}$
no cut	0.0004	0.019	0.013	0.013	0.0093
100	0.0005	0.031	0.022	0.021	0.015
300	0.0025	0.16	0.11	0.13	0.091
500	0.0070				
750	0.018				
1000	0.037				
1500	0.13				
2000	0.32				

Table 22: Expected statistical uncertainties for the polarization and spin correlation measurements in $b\bar{b}$ at the HL-LHC with a neutrino spin analyzer for different selection channels.

Quark	Polarization			
	Channel	Run 2		HL-LHC
		standard	parked	
s				(✓)
c	hadronic	(✓)		✓
	semileptonic	✓		✓
	mixed	(✓)		✓
b	inclusive	(✓)	(✓)	(✓)
	semi-inclusive	✓	✓	✓
	exclusive	✓	✓	✓

Quark	Spin Correlations			
	Channel	Run 2		HL-LHC
		standard	parked	
s				
c	hadronic			
	semileptonic			✓
	mixed			✓
b	inclusive/inclusive	(✓)	(✓)	(✓)
	semi-inclusive/semi-inclusive	✓	✓	✓
	exclusive/exclusive	✓	✓	✓
	inclusive/exclusive	(✓)	(✓)	(✓)
	inclusive/semi-inclusive	(✓)	(✓)	(✓)
	exclusive/semi-inclusive	✓	✓	✓

Table 23: The prospects in Run 2 and HL-LHC datasets for the different analysis channels examined. The top table is for polarization and the bottom is for spin correlations. Check marks indicate that a measurement is expected to be possible, and crossed check marks indicate borderline cases. Parentheses around a check mark indicate low sample purity, under 10%. The “parked” column refers to the CMS parked b -hadron dataset [36, 37].

actual performance of the corresponding analyses may be worse because of neglected backgrounds or effects of unfolding. On the other hand, improvements in the reconstruction of electrons within jets to make them comparable to muons would enhance the performance. Advanced machine learning techniques that have been entering the field recently can also boost the performance by improving object identification and reconstruction and/or background rejection. Finally, new trigger paths that might be deployed in future runs of the LHC have the potential to improve the statistics of all of the proposed analyses.

Since the angular distribution coefficients C_{ii} and C_{ij}^\pm that will be measured in the spin correlation analyses depend on the polarization retention factors r_L and r_T via eq. (4.12), the analyses proposed in this paper can be used to determine these factors for c and b quarks. By relying on spin correlation components allowed to be large by the symmetries of QCD (specifically c_{kk} , c_{nn} , c_{rr} , and c_{rk}),¹⁶ one can extract r_L and r_T using the (partly redundant) relations

$$r_L^2 = \frac{C_{kk}}{c_{kk}\alpha_+\alpha_-f}, \quad r_T^2 = \frac{C_{nn}}{c_{nn}\alpha_+\alpha_-f}, \quad r_T^2 = \frac{C_{rr}}{c_{rr}\alpha_+\alpha_-f}, \quad r_L r_T = \frac{C_{rk}^+}{2c_{rk}\alpha_+\alpha_-f}. \quad (7.1)$$

The measurements of r_L and r_T can lead to further understanding of the polarization transfer in QCD fragmentation and act as a test for different models of low-energy QCD phenomenology (e.g., ref. [35]). It will also be interesting to compare the values of r_L that will be obtained in these spin correlation measurements with those that will hopefully be obtained in polarization measurements of b and c quarks in $t\bar{t}$ [18] and $W+c$ [21] samples.

The polarization and spin correlation measurements can in principle also be utilized to probe for BSM contributions to $pp \rightarrow q\bar{q}$ processes, especially using the numerous components in which the SM contribution is expected to be small. Whether such searches can be competitive with other probes of the same BSM scenarios is a subject for another study.

Acknowledgments

This research was supported in part by the Israel Science Foundation (grants no. 780/17 and 1666/22) and the United States - Israel Binational Science Foundation (grant no. 2018257).

A Statistical Uncertainty Formulas

The angular distributions in eqs. (4.14), (4.15) and (4.16) are all of the form

$$\frac{1}{\sigma} \frac{d\sigma}{dX} = \frac{1}{2} (1 + cX) f(|X|), \quad (A.1)$$

where

$$X = \cos\theta_i^\pm, \quad \cos\theta_i^+ \cos\theta_j^-, \quad \cos\theta_i^+ \cos\theta_j^- \pm \cos\theta_j^+ \cos\theta_i^- \quad (A.2)$$

and

$$f(|X|) = 1, \quad \ln\left(\frac{1}{|X|}\right), \quad \cos^{-1}(|X|), \quad (A.3)$$

¹⁶In practice, c_{rk} happens to be small when p_T cuts are applied, as can be seen in tables 3 and 4.

respectively. We imagine extracting the value of c from the data with a χ^2 minimization procedure for a binned distribution of X . The χ^2 function is

$$\chi^2(c) = \sum_i \frac{[n_i - \frac{1}{2}(1 + cX_i) f(|X_i|) N \Delta X]^2}{\sigma_i^2}, \quad (\text{A.4})$$

where the summation is over bins of size ΔX , n_i is the number of events observed in bin i , X_i is the value of X in the middle of that bin, N is the total number of events, and

$$\sigma_i^2 \simeq n_i \simeq \frac{1}{2} (1 + cX_i) f(|X_i|) N \Delta X \quad (\text{A.5})$$

is the squared uncertainty of the expected number of events in bin i . Solving the minimization condition $d\chi^2/dc = 0$ for c and then propagating the statistical uncertainties of n_i , we find for the uncertainty of c :

$$\Delta c = \frac{1}{S(c)\sqrt{N}}, \quad (\text{A.6})$$

with

$$S^2(c) \simeq \frac{\Delta X}{2} \sum_i \frac{X_i^2}{1 + cX_i} f(|X_i|), \quad (\text{A.7})$$

where we assumed $n_i \gg 1$. In the limit of a large number of bins we can approximate the sum with an integral and obtain

$$S^2(c) \simeq \frac{1}{2} \int_{-1}^1 \frac{X^2}{1 + cX} f(|X|) dX = \int_0^1 \frac{X^2}{1 - c^2 X^2} f(X) dX. \quad (\text{A.8})$$

The uncertainties on the parameters B_i^\pm ($\equiv B$), C_{ii} , and $C_{ij}^\pm/2$ are then given by

$$\Delta B = \frac{1}{S_B(B)\sqrt{N}}, \quad (\text{A.9})$$

$$\Delta C_{ii} = \frac{1}{S_{C_{ii}}(C_{ii})\sqrt{N}}, \quad (\text{A.10})$$

$$\Delta(C_{ij}^\pm/2) = \frac{1}{S_{C_{ij}^\pm/2}(C_{ij}^\pm/2)\sqrt{N}}, \quad (\text{A.11})$$

where

$$S_B^2(B) \simeq \int_0^1 \frac{X^2}{1 - B^2 X^2} dX = \frac{\text{arctanh } B - B}{B^3}, \quad (\text{A.12})$$

$$S_{C_{ii}}^2(C_{ii}) \simeq \int_1^0 \frac{X^2}{1 - C_{ii}^2 X^2} \ln\left(\frac{1}{X}\right) dX = \frac{1}{9} + \frac{1}{4} C_{ii}^2 \Phi(C_{ii}^2, 2, \frac{5}{2}), \quad (\text{A.13})$$

$$\begin{aligned} S_{C_{ij}^\pm/2}^2(c) &\simeq \int_1^0 \frac{X^2}{1 - c^2 X^2} \cos^{-1}(X) dX \\ &= \frac{1}{4ic^3} \left[2 \text{Li}_2 \left(\frac{1}{(ic + \sqrt{1 - c^2})^2} \right) - 8 \text{Li}_2(\sqrt{1 - c^2} - ic) \right. \\ &\quad \left. + 2 \left(\pi + 2i \ln \left(\frac{\sqrt{1 - c^2} - 1}{c} \right) \right) \arcsin c - 4ic + \pi^2 \right], \end{aligned} \quad (\text{A.14})$$

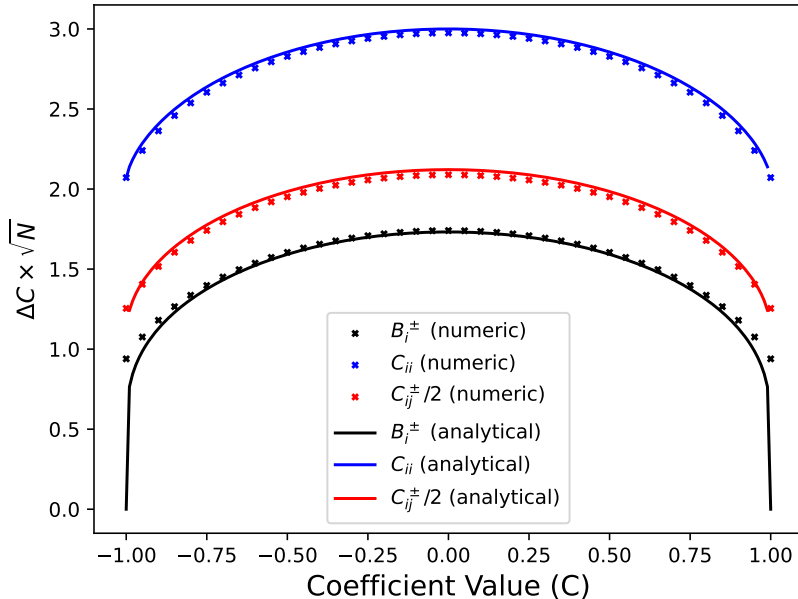


Figure 5: Statistical uncertainty (multiplied by \sqrt{N} , where N is the number of events) of the angular distribution coefficients B_i^\pm (black), C_{ii} (blue), and $C_{ij}^\pm/2$ (red) as a function of the coefficient values, calculated both analytically (solid curves) and numerically (dots). The analytical results are in the limit of an infinite number of bins, while the numerical (Monte Carlo) results are for 10 bins.

where the function Φ is the Lerch transcendent, Li_2 is the dilogarithm, and c in eq. (A.14) stands for $C_{ij}^\pm/2$.

In figure 5 we plot the uncertainties of the coefficients as a function of the coefficient values based on the analytic formulas in eqs. (A.12)–(A.14), which correspond to the limit of a large number of bins. We also show the results of a Monte Carlo simulation of a χ^2 minimization procedure with 10 bins. There is a good agreement between the two sets of results, except very close to $B = -1$ or 1 , where the analytical formula, which assumes infinitesimally small (but at the same time highly populated) bins, gives vanishing uncertainty. This happens because bins near $X = 1$ or -1 in these cases contain a vanishingly small fraction of events, making the uncertainty in those bins vanishingly small too, which in turn leads to a vanishingly small uncertainty in B . This situation is unphysical because measurements of X always have some uncertainty, ΔX , which prevents bins much smaller than ΔX from being useful.

While the polarization and spin correlation components (b_i^\pm, c_{ij}, c_ℓ) can in principle be anywhere in the range $[-1, 1]$, the polarization retention factors r_i and in many cases also the purity f or the spin analyzing powers α_\pm in eq. (4.12) will limit the angular distribution coefficients B_i^\pm, C_{ii} , and $C_{ij}^\pm/2$ to a smaller range of values. This, together with the flatness of the curves in figure 5 in the vicinity of zero, implies that the uncertainties can usually

be approximated by their values at zero. We have

$$S_B(0) = \frac{1}{\sqrt{3}}, \quad S_{C_{ii}}(0) = \frac{1}{3}, \quad S_{C_{ij}^{\pm}/2}(0) = \frac{\sqrt{2}}{3}, \quad (\text{A.15})$$

which leads to eq. (4.17).

References

- [1] W. Bernreuther, A. Brandenburg, Z. G. Si, and P. Uwer, “Top-Quark Spin Correlations at Hadron Colliders: Predictions at Next-to-Leading Order QCD,” *Phys. Rev. Lett.* **87** (2001) 242002, [arXiv:hep-ph/0107086](#).
- [2] W. Bernreuther, A. Brandenburg, Z. G. Si, and P. Uwer, “Top quark pair production and decay at hadron colliders,” *Nucl. Phys. B* **690** (2004) 81–137, [arXiv:hep-ph/0403035](#).
- [3] G. Mahlon and S. J. Parke, “Spin correlation effects in top quark pair production at the LHC,” *Phys. Rev. D* **81** (2010) 074024, [arXiv:1001.3422 \[hep-ph\]](#).
- [4] M. Baumgart and B. Tweedie, “Discriminating top-antitop resonances using azimuthal decay correlations,” *JHEP* **09** (2011) 049, [arXiv:1104.2043 \[hep-ph\]](#).
- [5] M. Baumgart and B. Tweedie, “A new twist on top quark spin correlations,” *JHEP* **03** (2013) 117, [arXiv:1212.4888 \[hep-ph\]](#).
- [6] M. Baumgart and B. Tweedie, “Transverse top quark polarization and the $t\bar{t}$ forward-backward asymmetry,” *JHEP* **08** (2013) 072, [arXiv:1303.1200 \[hep-ph\]](#).
- [7] W. Bernreuther and Z.-G. Si, “Top quark spin correlations and polarization at the LHC: Standard model predictions and effects of anomalous top chromo moments,” *Phys. Lett. B* **725** (2013) 115–122, [arXiv:1305.2066 \[hep-ph\]](#). [Erratum: *Phys. Lett. B* **744** (2015) 413–413].
- [8] W. Bernreuther, D. Heisler, and Z.-G. Si, “A set of top quark spin correlation and polarization observables for the LHC: Standard Model predictions and new physics contributions,” *JHEP* **12** (2015) 026, [arXiv:1508.05271 \[hep-ph\]](#).
- [9] A. Behring, M. Czakon, A. Mitov, A. S. Papanastasiou, and R. Poncelet, “Higher Order Corrections to Spin Correlations in Top Quark Pair Production at the LHC,” *Phys. Rev. Lett.* **123** no. 8, (2019) 082001, [arXiv:1901.05407 \[hep-ph\]](#).
- [10] Y. Afik and J. R. M. de Nova, “Entanglement and quantum tomography with top quarks at the LHC,” *Eur. Phys. J. Plus* **136** no. 9, (2021) 907, [arXiv:2003.02280 \[quant-ph\]](#).
- [11] C. Severi and E. Vryonidou, “Quantum entanglement and top spin correlations in SMEFT at higher orders,” *JHEP* **01** (2023) 148, [arXiv:2210.09330 \[hep-ph\]](#).
- [12] ATLAS Collaboration, G. Aad *et al.*, “Measurement of Spin Correlation in Top-Antitop Quark Events and Search for Top Squark Pair Production in pp Collisions at $\sqrt{s} = 8$ TeV Using the ATLAS Detector,” *Phys. Rev. Lett.* **114** no. 14, (2015) 142001, [arXiv:1412.4742 \[hep-ex\]](#).
- [13] ATLAS Collaboration, M. Aaboud *et al.*, “Measurements of top quark spin observables in $t\bar{t}$ events using dilepton final states in $\sqrt{s} = 8$ TeV pp collisions with the ATLAS detector,” *JHEP* **03** (2017) 113, [arXiv:1612.07004 \[hep-ex\]](#).

- [14] CMS Collaboration, V. Khachatryan *et al.*, “Measurements of $t\bar{t}$ spin correlations and top quark polarization using dilepton final states in pp collisions at $\sqrt{s} = 8$ TeV,” *Phys. Rev. D* **93** no. 5, (2016) 052007, [arXiv:1601.01107 \[hep-ex\]](#).
- [15] CMS Collaboration, A. M. Sirunyan *et al.*, “Measurement of the top quark polarization and $t\bar{t}$ spin correlations using dilepton final states in proton-proton collisions at $\sqrt{s} = 13$ TeV,” *Phys. Rev. D* **100** no. 7, (2019) 072002, [arXiv:1907.03729 \[hep-ex\]](#).
- [16] ATLAS Collaboration, M. Aaboud *et al.*, “Measurements of top-quark pair spin correlations in the $e\mu$ channel at $\sqrt{s} = 13$ TeV using pp collisions in the ATLAS detector,” *Eur. Phys. J. C* **80** no. 8, (2020) 754, [arXiv:1903.07570 \[hep-ex\]](#).
- [17] ATLAS Collaboration, G. Aad *et al.*, “Observation of quantum entanglement in top-quark pairs using the ATLAS detector,” [arXiv:2311.07288 \[hep-ex\]](#).
- [18] M. Galanti, A. Giammanco, Y. Grossman, Y. Kats, E. Stamou, and J. Zupan, “Heavy baryons as polarimeters at colliders,” *JHEP* **11** (2015) 067, [arXiv:1505.02771 \[hep-ph\]](#).
- [19] Y. Kats, “Measuring polarization of light quarks at ATLAS and CMS,” *Phys. Rev. D* **92** (2015) 071503, [arXiv:1505.06731 \[hep-ph\]](#).
- [20] Y. Kats, “Kinked tracks from Σ^+ baryons as a probe of light quark polarizations,” *JHEP* **07** (2023) 018, [arXiv:2301.06188 \[hep-ph\]](#).
- [21] Y. Kats, “Measuring c -quark polarization in $W+c$ samples at ATLAS and CMS,” *JHEP* **11** (2016) 011, [arXiv:1512.00438 \[hep-ph\]](#).
- [22] T. Mannel and G. A. Schuler, “Semileptonic decays of bottom baryons at LEP,” *Phys. Lett. B* **279** (1992) 194–200.
- [23] F. E. Close, J. G. Körner, R. J. N. Phillips, and D. J. Summers, “Report of the b-fragmentation working group. Section 5: b polarization at LEP,” *J. Phys.* **G18** (1992) 1703.
- [24] A. F. Falk and M. E. Peskin, “Production, decay, and polarization of excited heavy hadrons,” *Phys. Rev. D* **49** (1994) 3320–3332, [arXiv:hep-ph/9308241](#).
- [25] ALEPH Collaboration, D. Buskulic *et al.*, “Measurement of the Λ_b polarization in Z decays,” *Phys. Lett. B* **365** (1996) 437–447.
- [26] OPAL Collaboration, G. Abbiendi *et al.*, “Measurement of the average polarization of b baryons in hadronic Z^0 decays,” *Phys. Lett. B* **444** (1998) 539–554, [arXiv:hep-ex/9808006](#).
- [27] DELPHI Collaboration, P. Abreu *et al.*, “ Λ_b polarization in Z^0 decays at LEP,” *Phys. Lett. B* **474** (2000) 205–222.
- [28] ALEPH Collaboration, D. Buskulic *et al.*, “Measurement of Λ polarization from Z decays,” *Phys. Lett. B* **374** (1996) 319–330.
- [29] ALEPH Collaboration, “Update of Λ polarization from Z decays,” Tech. Rep. CERN-OPEN-99-328, CERN, Geneva, 1997. <http://cds.cern.ch/record/407920>.
- [30] OPAL Collaboration, K. Ackerstaff *et al.*, “Polarization and forward-backward asymmetry of Λ baryons in hadronic Z^0 decays,” *Eur. Phys. J. C* **2** (1998) 49–59, [arXiv:hep-ex/9708027](#).
- [31] LHCb Collaboration, R. Aaij *et al.*, “Measurements of the $\Lambda_b^0 \rightarrow J/\psi\Lambda$ decay amplitudes

- and the Λ_b^0 polarisation in pp collisions at $\sqrt{s} = 7$ TeV,” *Phys. Lett. B* **724** (2013) 27–35, [arXiv:1302.5578 \[hep-ex\]](#).
- [32] LHCb Collaboration, R. Aaij *et al.*, “Measurement of the $\Lambda_b^0 \rightarrow J/\psi \Lambda$ angular distribution and the Λ_b^0 polarisation in pp collisions,” *JHEP* **06** (2020) 110, [arXiv:2004.10563 \[hep-ex\]](#).
- [33] CMS Collaboration, A. M. Sirunyan *et al.*, “Measurement of the Λ_b polarization and angular parameters in $\Lambda_b \rightarrow J/\psi \Lambda$ decays from pp collisions at $\sqrt{s} = 7$ and 8 TeV,” *Phys. Rev. D* **97** no. 7, (2018) 072010, [arXiv:1802.04867 \[hep-ex\]](#).
- [34] K. Chen, G. R. Goldstein, R. L. Jaffe, and X.-D. Ji, “Probing quark fragmentation functions for spin-1/2 baryon production in unpolarized e^+e^- annihilation,” *Nucl. Phys. B* **445** (1995) 380–398, [arXiv:hep-ph/9410337](#).
- [35] A. Adamov and G. R. Goldstein, “Excited state contributions to the heavy baryon fragmentation functions in a quark-diquark model,” *Phys. Rev. D* **64** (2001) 014021, [arXiv:hep-ph/0009300](#).
- [36] CMS Collaboration, “Recording and reconstructing 10 billion unbiased b hadron decays in CMS,” Tech. Rep. CMS-DP-2019-043, CERN, Geneva, 2019. <https://cds.cern.ch/record/2704495>.
- [37] CMS Collaboration, R. Bainbridge, “Recording and reconstructing 10 billion unbiased b hadron decays in CMS,” *EPJ Web Conf.* **245** (2020) 01025.
- [38] R. Alonso, C. Fraser-Taliente, C. Hays, and M. Spannowsky, “Prospects for direct CP tests of $hq\bar{q}$ interactions,” *JHEP* **08** (2021) 167, [arXiv:2105.06879 \[hep-ph\]](#).
- [39] M. Stratmann and W. Vogelsang, “Next-to-leading order evolution of polarized and unpolarized fragmentation functions,” *Nucl. Phys. B* **496** (1997) 41–65, [arXiv:hep-ph/9612250](#).
- [40] D. de Florian, M. Stratmann, and W. Vogelsang, “QCD analysis of unpolarized and polarized Λ -baryon production in leading and next-to-leading order,” *Phys. Rev. D* **57** (1998) 5811–5824, [arXiv:hep-ph/9711387](#).
- [41] G. Gustafson and J. Hakkinen, “ Λ -polarization in e^+e^- -annihilation at the Z^0 pole,” *Phys. Lett. B* **303** (1993) 350–354.
- [42] Particle Data Group Collaboration, R. L. Workman and Others, “Review of Particle Physics,” *PTEP* **2022** (2022) 083C01.
- [43] A. V. Manohar and M. B. Wise, “Inclusive semileptonic B and polarized Λ_b decays from QCD,” *Phys. Rev. D* **49** (1994) 1310–1329, [arXiv:hep-ph/9308246](#).
- [44] M. Lisovskyi, A. Verbytskyi, and O. Zenaiev, “Combined analysis of charm-quark fragmentation-fraction measurements,” *Eur. Phys. J. C* **76** no. 7, (2016) 397, [arXiv:1509.01061 \[hep-ex\]](#).
- [45] LHCb Collaboration, R. Aaij *et al.*, “Amplitude analysis of the $\Lambda_c^+ \rightarrow pK^-\pi^+$ decay and Λ_c^+ baryon polarization measurement in semileptonic beauty hadron decays,” *Phys. Rev. D* **108** no. 1, (2023) 012023, [arXiv:2208.03262 \[hep-ex\]](#).
- [46] A. Czarnecki and M. Jezabek, “Distributions of leptons in decays of polarized heavy quarks,” *Nucl. Phys. B* **427** (1994) 3–21, [arXiv:hep-ph/9402326](#).

- [47] T. Sjöstrand, S. Ask, J. R. Christiansen, R. Corke, N. Desai, P. Ilten, S. Mrenna, S. Prestel, C. O. Rasmussen, and P. Z. Skands, “An introduction to PYTHIA 8.2,” *Comput. Phys. Commun.* **191** (2015) 159–177, [arXiv:1410.3012 \[hep-ph\]](#).
- [48] S. Albino, B. A. Kniehl, and G. Kramer, “AKK Update: Improvements from New Theoretical Input and Experimental Data,” *Nucl. Phys. B* **803** (2008) 42–104, [arXiv:0803.2768 \[hep-ph\]](#).
- [49] ATLAS Collaboration, M. Aaboud *et al.*, “Measurements of charge and CP asymmetries in b -hadron decays using top-quark events collected by the ATLAS detector in pp collisions at $\sqrt{s} = 8$ TeV,” *JHEP* **02** (2017) 071, [arXiv:1610.07869 \[hep-ex\]](#).
- [50] CMS Collaboration, A. Tumasyan *et al.*, “A new calibration method for charm jet identification validated with proton-proton collision events at $\sqrt{s} = 13$ TeV,” *JINST* **17** no. 03, (2022) P03014, [arXiv:2111.03027 \[hep-ex\]](#).
- [51] CMS Collaboration, A. Tumasyan *et al.*, “Measurement of the production cross section for a W boson in association with a charm quark in proton-proton collisions at $\sqrt{s} = 13$ TeV,” [arXiv:2308.02285 \[hep-ex\]](#).
- [52] M. Cacciari, G. P. Salam, and G. Soyez, “The anti- k_t jet clustering algorithm,” *JHEP* **04** (2008) 063, [arXiv:0802.1189 \[hep-ph\]](#).
- [53] M. Cacciari, G. P. Salam, and G. Soyez, “FastJet User Manual,” *Eur. Phys. J. C* **72** (2012) 1896, [arXiv:1111.6097 \[hep-ph\]](#).
- [54] ALEPH Collaboration, A. Heister *et al.*, “Study of the fragmentation of b quarks into B mesons at the Z peak,” *Phys. Lett. B* **512** (2001) 30–48, [arXiv:hep-ex/0106051](#).
- [55] DELPHI Collaboration, J. Abdallah *et al.*, “A study of the b-quark fragmentation function with the DELPHI detector at LEP I and an averaged distribution obtained at the Z Pole,” *Eur. Phys. J. C* **71** (2011) 1557, [arXiv:1102.4748 \[hep-ex\]](#).
- [56] OPAL Collaboration, G. Abbiendi *et al.*, “Inclusive analysis of the b quark fragmentation function in Z decays at LEP,” *Eur. Phys. J. C* **29** (2003) 463–478, [arXiv:hep-ex/0210031](#).
- [57] SLD Collaboration, K. Abe *et al.*, “Measurement of the b-quark fragmentation function in Z^0 decays,” *Phys. Rev. D* **65** (2002) 092006, [arXiv:hep-ex/0202031](#). [Erratum: *Phys. Rev. D* **66** (2002) 079905].
- [58] ATLAS Collaboration, G. Aad *et al.*, “Measurements of jet observables sensitive to b-quark fragmentation in $t\bar{t}$ events at the LHC with the ATLAS detector,” *Phys. Rev. D* **106** no. 3, (2022) 032008, [arXiv:2202.13901 \[hep-ex\]](#).
- [59] ATLAS Collaboration, G. Aad *et al.*, “Measurement of b-quark fragmentation properties in jets using the decay $B^\pm \rightarrow J/\psi K^\pm$ in pp collisions at $\sqrt{s} = 13$ TeV with the ATLAS detector,” *JHEP* **12** (2021) 131, [arXiv:2108.11650 \[hep-ex\]](#).
- [60] CMS Collaboration, “Measurement of the shape of the b quark fragmentation function using charmed mesons produced inside b jets from $t\bar{t}$ pair decays,” Tech. Rep. CMS-PAS-TOP-18-012, CERN, Geneva, 2021. <https://cds.cern.ch/record/2771694>.
- [61] OPAL Collaboration, K. Ackerstaff *et al.*, “Measurement of $f(c \rightarrow D^{*+} X)$, $f(b \rightarrow D^{*+} X)$ and $\Gamma_{c\bar{c}}/\Gamma_{\text{had}}$ using $D^{*\pm}$ mesons,” *Eur. Phys. J. C* **1** (1998) 439–459, [arXiv:hep-ex/9708021](#).
- [62] ALEPH Collaboration, R. Barate *et al.*, “Study of charm production in Z decays,” *Eur. Phys. J. C* **16** (2000) 597–611, [arXiv:hep-ex/9909032](#).

- [63] M. Cacciari, P. Nason, and C. Oleari, “A study of heavy flavoured meson fragmentation functions in e^+e^- annihilation,” *JHEP* **04** (2006) 006, [arXiv:hep-ph/0510032](#).
- [64] S. Dambach, U. Langenegger, and A. Starodumov, “Neutrino reconstruction with topological information,” *Nucl. Instrum. Meth. A* **569** (2006) 824–828, [arXiv:hep-ph/0607294](#).
- [65] LHCb Collaboration, R. Aaij *et al.*, “Determination of the quark coupling strength $|V_{ub}|$ using baryonic decays,” *Nature Phys.* **11** (2015) 743–747, [arXiv:1504.01568](#) [[hep-ex](#)].
- [66] LHCb Collaboration, R. Aaij *et al.*, “First Observation of the Decay $B_s^0 \rightarrow K^- \mu^+ \nu_\mu$ and a Measurement of $|V_{ub}|/|V_{cb}|$,” *Phys. Rev. Lett.* **126** no. 8, (2021) 081804, [arXiv:2012.05143](#) [[hep-ex](#)].
- [67] G. Ciezarek, A. Lupato, M. Rotondo, and M. Vesterinen, “Reconstruction of semileptonically decaying beauty hadrons produced in high energy pp collisions,” *JHEP* **02** (2017) 021, [arXiv:1611.08522](#) [[hep-ex](#)].
- [68] U. Fano, “Pairs of two-level systems,” *Rev. Mod. Phys.* **55** (1983) 855–874.
- [69] W. G. D. Dharmaratna and G. R. Goldstein, “Single quark polarization in quantum chromodynamics subprocesses,” *Phys. Rev. D* **53** (1996) 1073–1086.
- [70] W. Bernreuther, A. Brandenburg, and P. Uwer, “Transverse polarization of top quark pairs at the Tevatron and the Large Hadron Collider,” *Phys. Lett. B* **368** (1996) 153–162, [arXiv:hep-ph/9510300](#).
- [71] J. Alwall, R. Frederix, S. Frixione, V. Hirschi, F. Maltoni, O. Mattelaer, H. S. Shao, T. Stelzer, P. Torrielli, and M. Zaro, “The automated computation of tree-level and next-to-leading order differential cross sections, and their matching to parton shower simulations,” *JHEP* **07** (2014) 079, [arXiv:1405.0301](#) [[hep-ph](#)].
- [72] P. Artoisenet, R. Frederix, O. Mattelaer, and R. Rietkerk, “Automatic spin-entangled decays of heavy resonances in Monte Carlo simulations,” *JHEP* **03** (2013) 015, [arXiv:1212.3460](#) [[hep-ph](#)].
- [73] D. Buarque Franzosi, O. Mattelaer, R. Ruiz, and S. Shil, “Automated predictions from polarized matrix elements,” *JHEP* **04** (2020) 082, [arXiv:1912.01725](#) [[hep-ph](#)].
- [74] ATLAS Collaboration, “Expected performance of the ATLAS detector at the High-Luminosity LHC,” Tech. Rep. ATL-PHYS-PUB-2019-005, CERN, Geneva, 2019. <https://cds.cern.ch/record/2655304>.
- [75] CMS Collaboration, “The Phase-2 Upgrade of the CMS Data Acquisition and High Level Trigger,” Tech. Rep. CERN-LHCC-2021-007, CMS-TDR-022, CERN, Geneva, 2021. <https://cds.cern.ch/record/2759072>.
- [76] ATLAS Collaboration, R. E. Owen, “The ATLAS Trigger System,”. <https://cds.cern.ch/record/2302730>.
- [77] ATLAS Collaboration, G. Aad *et al.*, “Performance of the ATLAS muon triggers in Run 2,” *JINST* **15** no. 09, (2020) P09015, [arXiv:2004.13447](#) [[physics.ins-det](#)].
- [78] ATLAS Collaboration, G. Aad *et al.*, “Configuration and performance of the ATLAS b -jet triggers in Run 2,” *Eur. Phys. J. C* **81** no. 12, (2021) 1087, [arXiv:2106.03584](#) [[hep-ex](#)].
- [79] ATLAS Collaboration, G. Aad *et al.*, “ K_S^0 and Λ production in pp interactions at $\sqrt{s} = 0.9$

- and 7 TeV measured with the ATLAS detector at the LHC,” *Phys. Rev. D* **85** (2012) 012001, [arXiv:1111.1297 \[hep-ex\]](#).
- [80] ATLAS Collaboration, G. Aad *et al.*, “Measurement of the Λ_b^0 lifetime and mass in the ATLAS experiment,” *Phys. Rev. D* **87** no. 3, (2013) 032002, [arXiv:1207.2284 \[hep-ex\]](#).
- [81] ATLAS Collaboration, G. Aad *et al.*, “Measurement of the parity-violating asymmetry parameter α_b and the helicity amplitudes for the decay $\Lambda_b^0 \rightarrow J/\psi \Lambda^0$ with the ATLAS detector,” *Phys. Rev. D* **89** no. 9, (2014) 092009, [arXiv:1404.1071 \[hep-ex\]](#).
- [82] ATLAS Collaboration, G. Aad *et al.*, “Measurement of K_S^0 and Λ^0 production in $t\bar{t}$ dileptonic events in pp collisions at $\sqrt{s} = 7$ TeV with the ATLAS detector,” *Eur. Phys. J. C* **79** no. 12, (2019) 1017, [arXiv:1907.10862 \[hep-ex\]](#).
- [83] CMS Collaboration, V. Khachatryan *et al.*, “Strange Particle Production in pp Collisions at $\sqrt{s} = 0.9$ and 7 TeV,” *JHEP* **05** (2011) 064, [arXiv:1102.4282 \[hep-ex\]](#).
- [84] CMS Collaboration, A. M. Sirunyan *et al.*, “Strange hadron production in pp and pPb collisions at $\sqrt{s_{NN}} = 5.02$ TeV,” *Phys. Rev. C* **101** no. 6, (2020) 064906, [arXiv:1910.04812 \[hep-ex\]](#).
- [85] CMS Collaboration, A. M. Sirunyan *et al.*, “Study of excited Λ_b^0 states decaying to $\Lambda_b^0 \pi^+ \pi^-$ in proton-proton collisions at $\sqrt{s} = 13$ TeV,” *Phys. Lett. B* **803** (2020) 135345, [arXiv:2001.06533 \[hep-ex\]](#).
- [86] CMS Collaboration, A. M. Sirunyan *et al.*, “Observation of a New Excited Beauty Strange Baryon Decaying to $\Xi_b^- \pi^+ \pi^-$,” *Phys. Rev. Lett.* **126** no. 25, (2021) 252003, [arXiv:2102.04524 \[hep-ex\]](#).
- [87] ATLAS Collaboration, “Performance of the reconstruction of large impact parameter tracks in the ATLAS inner detector,” Tech. Rep. ATL-PHYS-PUB-2017-014, CERN, Geneva, 2017. <https://cds.cern.ch/record/2275635>.
- [88] ATLAS Collaboration, “Performance of vertex reconstruction algorithms for detection of new long-lived particle decays within the ATLAS inner detector,” Tech. Rep. ATL-PHYS-PUB-2019-013, CERN, Geneva, 2019. <https://cds.cern.ch/record/2669425>.
- [89] ATLAS Collaboration, G. Aad *et al.*, “Performance of the reconstruction of large impact parameter tracks in the inner detector of ATLAS,” [arXiv:2304.12867 \[hep-ex\]](#).
- [90] ATLAS Collaboration, M. Aaboud *et al.*, “Search for long-lived, massive particles in events with displaced vertices and missing transverse momentum in $\sqrt{s} = 13$ TeV pp collisions with the ATLAS detector,” *Phys. Rev. D* **97** no. 5, (2018) 052012, [arXiv:1710.04901 \[hep-ex\]](#).
- [91] ATLAS Collaboration, G. Aad *et al.*, “Search for heavy neutral leptons in decays of W bosons produced in 13 TeV pp collisions using prompt and displaced signatures with the ATLAS detector,” *JHEP* **10** (2019) 265, [arXiv:1905.09787 \[hep-ex\]](#).
- [92] ATLAS Collaboration, G. Aad *et al.*, “Search for displaced vertices of oppositely charged leptons from decays of long-lived particles in pp collisions at $\sqrt{s} = 13$ TeV with the ATLAS detector,” *Phys. Lett. B* **801** (2020) 135114, [arXiv:1907.10037 \[hep-ex\]](#).
- [93] ATLAS Collaboration, G. Aad *et al.*, “Search for long-lived neutral particles produced in pp collisions at $\sqrt{s} = 13$ TeV decaying into displaced hadronic jets in the ATLAS inner detector and muon spectrometer,” *Phys. Rev. D* **101** no. 5, (2020) 052013, [arXiv:1911.12575 \[hep-ex\]](#).

- [94] ATLAS Collaboration, G. Aad *et al.*, “Search for long-lived, massive particles in events with a displaced vertex and a muon with large impact parameter in pp collisions at $\sqrt{s} = 13$ TeV with the ATLAS detector,” *Phys. Rev. D* **102** no. 3, (2020) 032006, [arXiv:2003.11956 \[hep-ex\]](#).
- [95] ATLAS Collaboration, G. Aad *et al.*, “Search for Displaced Leptons in $\sqrt{s} = 13$ TeV pp Collisions with the ATLAS Detector,” *Phys. Rev. Lett.* **127** no. 5, (2021) 051802, [arXiv:2011.07812 \[hep-ex\]](#).
- [96] ATLAS Collaboration, G. Aad *et al.*, “Search for exotic decays of the Higgs boson into long-lived particles in pp collisions at $\sqrt{s} = 13$ TeV using displaced vertices in the ATLAS inner detector,” *JHEP* **11** (2021) 229, [arXiv:2107.06092 \[hep-ex\]](#).
- [97] ATLAS Collaboration, G. Aad *et al.*, “Search for long-lived, massive particles in events with displaced vertices and multiple jets in pp collisions at $\sqrt{s} = 13$ TeV with the ATLAS detector,” *JHEP* **2306** (2023) 200, [arXiv:2301.13866 \[hep-ex\]](#).
- [98] ATLAS Collaboration, T. Strebler, “Expected tracking performance of the ATLAS Phase-II Inner Tracker Upgrade,” *PoS ICHEP2022* (2022) 665.
- [99] CMS Collaboration, A. M. Sirunyan *et al.*, “Production of Λ_c^+ baryons in proton-proton and lead-lead collisions at $\sqrt{s_{NN}} = 5.02$ TeV,” *Phys. Lett. B* **803** (2020) 135328, [arXiv:1906.03322 \[hep-ex\]](#).
- [100] CMS Collaboration, A. Tumasyan *et al.*, “Study of charm hadronization with prompt Λ_c^+ baryons in proton-proton and lead-lead collisions at $\sqrt{s_{NN}} = 5.02$ TeV,” [arXiv:2307.11186 \[nucl-ex\]](#).
- [101] ATLAS Collaboration, “CP-violation measurement prospects in the $B_s^0 \rightarrow J/\psi\phi$ channel with the upgraded ATLAS detector at the HL-LHC,” Tech. Rep. ATL-PHYS-PUB-2018-041, CERN, Geneva, 2018. <https://cds.cern.ch/record/2649881>.
- [102] ATLAS Collaboration, “Prospects for lepton flavour violation measurements in $\tau \rightarrow 3\mu$ decays with the ATLAS detector at the HL-LHC,” Tech. Rep. ATL-PHYS-PUB-2018-032, CERN, Geneva, 2018. <https://cds.cern.ch/record/2647956>.
- [103] ATLAS Collaboration, “Evaluation of theoretical uncertainties for simplified template cross section measurements of V -associated production of the Higgs boson,” Tech. Rep. ATL-PHYS-PUB-2018-035, CERN, Geneva, 2018. <https://cds.cern.ch/record/2649241>.
- [104] CMS Collaboration, “Measurement of rare $B \rightarrow \mu^+\mu^-$ decays with the Phase-2 upgraded CMS detector at the HL-LHC,” Tech. Rep. CMS-PAS-FTR-18-013, CERN, Geneva, 2018. <https://cds.cern.ch/record/2650545>.
- [105] CMS Collaboration, “Study of the expected sensitivity to the P'_5 parameter in the $B^0 \rightarrow K^{*0}\mu^+\mu^-$ decay at the HL-LHC,” Tech. Rep. CMS-PAS-FTR-18-033, CERN, Geneva, 2018. <https://cds.cern.ch/record/2651298>.
- [106] ATLAS Collaboration, G. Aad *et al.*, “Performance of b -Jet Identification in the ATLAS Experiment,” *JINST* **11** no. 04, (2016) P04008, [arXiv:1512.01094 \[hep-ex\]](#).
- [107] CMS Collaboration, A. M. Sirunyan *et al.*, “Identification of heavy-flavour jets with the CMS detector in pp collisions at 13 TeV,” *JINST* **13** no. 05, (2018) P05011, [arXiv:1712.07158 \[physics.ins-det\]](#).

- [108] ATLAS Collaboration, “Calibration of the b -tagging efficiency on charm jets using a sample of $W+c$ events with $\sqrt{s} = 13$ TeV ATLAS data,” Tech. Rep. ATLAS-CONF-2018-055, CERN, Geneva, 2018. <https://cds.cern.ch/record/2652195>.
- [109] ATLAS Collaboration, G. Aad *et al.*, “ATLAS flavour-tagging algorithms for the LHC Run 2 pp collision dataset,” *Eur. Phys. J. C* **83** no. 7, (2023) 681, [arXiv:2211.16345](https://arxiv.org/abs/2211.16345) [[physics.data-an](#)].
- [110] ATLAS Collaboration, M. Aaboud *et al.*, “Search for long-lived charginos based on a disappearing-track signature in pp collisions at $\sqrt{s} = 13$ TeV with the ATLAS detector,” *JHEP* **06** (2018) 022, [arXiv:1712.02118](https://arxiv.org/abs/1712.02118) [[hep-ex](#)].
- [111] ATLAS Collaboration, G. Aad *et al.*, “Search for long-lived charginos based on a disappearing-track signature using 136 fb^{-1} of pp collisions at $\sqrt{s} = 13$ TeV with the ATLAS detector,” *Eur. Phys. J. C* **82** no. 7, (2022) 606, [arXiv:2201.02472](https://arxiv.org/abs/2201.02472) [[hep-ex](#)].
- [112] CMS Collaboration, A. M. Sirunyan *et al.*, “Searches for physics beyond the standard model with the M_{T2} variable in hadronic final states with and without disappearing tracks in proton-proton collisions at $\sqrt{s} = 13$ TeV,” *Eur. Phys. J. C* **80** no. 1, (2020) 3, [arXiv:1909.03460](https://arxiv.org/abs/1909.03460) [[hep-ex](#)].
- [113] CMS Collaboration, A. M. Sirunyan *et al.*, “Search for disappearing tracks in proton-proton collisions at $\sqrt{s} = 13$ TeV,” *Phys. Lett. B* **806** (2020) 135502, [arXiv:2004.05153](https://arxiv.org/abs/2004.05153) [[hep-ex](#)].
- [114] CMS Collaboration, A. Hayrapetyan *et al.*, “Search for supersymmetry in final states with disappearing tracks in proton-proton collisions at $\sqrt{s} = 13$ TeV,” [arXiv:2309.16823](https://arxiv.org/abs/2309.16823) [[hep-ex](#)].
- [115] CMS Collaboration, S. Chatrchyan *et al.*, “Identification of b -quark jets with the CMS experiment,” *JINST* **8** (2013) P04013, [arXiv:1211.4462](https://arxiv.org/abs/1211.4462) [[hep-ex](#)].
- [116] ATLAS Collaboration, G. Aad *et al.*, “Measurement of the top-quark mass using a leptonic invariant mass in pp collisions at $\sqrt{s} = 13$ TeV with the ATLAS detector,” *JHEP* **06** (2023) 019, [arXiv:2209.00583](https://arxiv.org/abs/2209.00583) [[hep-ex](#)].
- [117] HFLAV Collaboration, Y. Amhis *et al.*, “Averages of b -hadron, c -hadron, and τ -lepton properties as of summer 2014,” [arXiv:1412.7515](https://arxiv.org/abs/1412.7515) [[hep-ex](#)].
- [118] CMS Collaboration, A. Hayrapetyan *et al.*, “Development of the CMS detector for the CERN LHC Run 3,” [arXiv:2309.05466](https://arxiv.org/abs/2309.05466) [[physics.ins-det](#)].